

1 **Long-read and chromosome-scale assembly of the**
2 **hexaploid wheat genome achieves high resolution for**
3 **research and breeding**

4

5 Jean-Marc Aury^{1,*}, Stefan Engelen¹, Benjamin Istace¹, Cécile Monat², Pauline
6 Lasserre-Zuber², Caroline Belser¹, Corinne Cruaud³, Hélène Rimbert², Philippe
7 Leroy², Sandrine Arribat⁴, Isabelle Dufau⁴, Arnaud Bellec⁴, David Grimbichler⁵,
8 Nathan Papon², Etienne Paux², Marion Ranoux², Adriana Alberti^{1,6}, Patrick Wincker¹,
9 Frédéric Choulet^{2,*}

10

11 * corresponding authors

12

13

14 ¹ Génomique Métabolique, Genoscope, Institut François Jacob, CEA, CNRS, Univ
15 Evry, Université Paris-Saclay, 91057 Evry, France

16 ² GDEC, Université Clermont Auvergne, INRAE, UMR1095, 63000 Clermont-
17 Ferrand, France

18 ³ Commissariat à l'Energie Atomique (CEA), Institut François Jacob, Genoscope, F-
19 91057 Evry, France

20 ⁴ INRAE, CNRGV French Plant Genomic Resource Center, F-31320, Castanet
21 Tolosan, France

22 ⁵ Mésocentre Clermont Auvergne, DOSI / Bâtiment Turing, 7 avenue Blaise Pascal,
23 63178 Aubière CEDEX

24 ⁶ Current address: Université Paris-Saclay, CEA, CNRS, Institute for Integrative
25 Biology of the Cell (I2BC), 91198, Gif-sur-Yvette, France.

26 Abstract

27 The sequencing of the wheat (*Triticum aestivum*) genome has been a methodological
28 challenge for many years due to its large size (15.5 Gb), repeat content, and hexaploidy.
29 Many initiatives aiming at obtaining a reference genome of cultivar Chinese Spring have
30 been launched in the past years and it was achieved in 2018 as the result of a huge effort to
31 combine short-read sequencing with many other resources. Reference-quality genome
32 assemblies were then produced for other accessions but the rapid evolution of sequencing
33 technologies offers opportunities to reach high-quality standards at lower cost. Here, we
34 report on an optimized procedure based on long-reads produced on the ONT (Oxford
35 Nanopore Technology) PromethION device to assemble the genome of the French bread
36 wheat cultivar Renan. We provide the most contiguous and complete chromosome-scale
37 assembly of a bread wheat genome to date. Coupled with an annotation based on RNA-Seq
38 data, this resource will be valuable for the crop community and will facilitate the rapid
39 selection of agronomically important traits. We also provide a framework to generate high-
40 quality assemblies of complex genomes using ONT.

41

42 Introduction

43 Bread wheat (*Triticum aestivum*) is among the most important cereal crops and a better
44 knowledge in the area of wheat genomics is needed to face the main challenge of ensuring
45 food security to a growing population in the context of climate change. Improving productivity
46 requires both that local producers adapt their practices to increase their climate resilience
47 and a better understanding of the wheat production systems. In this context, a better
48 knowledge of the wheat genome and its gene content, but also the sequencing of numerous
49 accessions, are essential.

50 However, the genome of bread wheat is particularly characterized by its complexity. Indeed,
51 this hexaploid genome is the result of two interspecific hybridization events. The earliest
52 cultivated wheat was diploid, but humans have intensified the cultivation of polyploid
53 species. Recent studies show that these polyploid species appear to be advantaged by their
54 genomic plasticity[1]. Indeed, modifications of the gene space and related elements are
55 buffered by the polyploid nature of wheat and open a wider field to selection. Bread wheat is
56 composed of three subgenomes A, B and D derived from three ancestral diploid species that
57 diverged between 2.5 and 6 million years ago[2].

58 The wheat genome is one of the largest among sequenced plant genomes (15.5 Gb), mainly
59 composed of repetitive sequences (ca. >85%), and contains many homoeologous regions
60 between the three subgenomes (A, B and D). Repetitive sequences and polyploidy pose
61 serious challenges in the generation of genome assemblies. The adventure of sequencing

62 the hexaploid wheat genome began in 2005 with the creation of the International Wheat
63 Genome Sequencing Consortium (IWGSC)[3]. With the advent of sequencing technologies,
64 the wheat genome has been competitively sequenced several times[4–6]. The first
65 reference-quality genome sequence with a comprehensive annotation was published by the
66 IWGSC in August 2018[7] for the accession Chinese Spring (CS). This assembly represents
67 a tremendous resource for the scientific community and offers the promise of facilitating and
68 accelerating breeding efforts.

69 More recently, fifteen genomes of hexaploid wheat have been published[8] which represents
70 a new step in the knowledge of the wheat model. Ten of these new wheat genomes have
71 been assembled at the chromosome level, allowing for comparative analysis on a scale that
72 was previously impossible. While being a valuable and highly validated resource using
73 multiple technologies, these assemblies were produced using short-read technologies and
74 therefore may contain a higher number of gaps compared to genomes assembled with long
75 reads[9–13]. In 2017, an assembly of the CS genome using long-reads was produced[5],
76 although not annotated, highlighting the added-value of long-reads in such complex
77 genomes. By accumulating long-read assemblies, the scientific community is now aware of
78 the flaw in short-read strategies. Indeed they underestimate the repetitive content of the
79 genome and more importantly can lack tandemly duplicated genes[14,15]. Several years
80 ago, Pacific Biosciences (PACBIO) and Oxford Nanopore (ONT) sequencing technologies
81 were commercialized with the promise to sequence long DNA fragments and revolutionize
82 complex genome assemblies.

83 Here, we report the first hexaploid wheat genome based on ONT long-reads. We sequenced
84 the genome of the French variety Renan, one of the most used varieties in organic farming.
85 The Renan genome carries multiple resistance genes against fungal pathogens (leaf rust,
86 stem rust, yellow rust, eyespot) originating from introgression of DNA regions coming from
87 the wild species *Aegilops ventricosa*. We used the PromethION device and organized the
88 assembled contigs at the chromosome scale using optical maps (BioNano Genomics, BNG)
89 and Hi-C libraries (Arima Genomics, AG). This assembly has a contig N50 of 2.2 Mb, which
90 is a 30-fold improvement over existing chromosome-scale assemblies.

91

92 Results

93 Genome sequencing and optical maps

94 We sequenced genomic DNA using 20 ONT flow cells (2 MinION and 18 PromethION)
95 which produced 12M reads representing 1.1 Tb. All the reads were originally base called
96 using the guppy 2.0 software, but given the improvement of guppy software during our

97 project, we decided to call bases using a newer version of the guppy software (version 3.6
98 with High Accuracy setting). This dataset represented a coverage of 63x of the hexaploid
99 wheat genome and the read N50 was of 24.6kb. More importantly, we got 3.1M reads larger
100 than 50kb representing a 14x genome coverage (Table S1). In addition, we generated
101 Illumina short-reads and long-range data for respectively polishing and organizing nanopore
102 contigs. We produced an optical map using the Saphyr instrument commercialized by
103 Bionano Genomics (BNG). High molecular weight DNA was extracted and labeled using the
104 Direct Label and Stain Chemistry (DLS) with the DLE-1 enzyme. The DLE-1 optical map was
105 assembled using proprietary tools provided by BNG and had a cumulative size of 14.9 Gb
106 with an N50 of 37.5 Mb (Table S2). Four Hi-C libraries from two biological replicates were
107 prepared using the Arima Genomics protocol and sequenced on an Illumina sequencer to
108 reach 537 Gb i.e., a depth of 35x. We used a sample of 240 million read pairs (72 Gb, 5x) to
109 build a Hi-C map.

110 **Genome assembly**

111 Since the dataset was too large for many long-read assemblers, we sampled a 30x coverage
112 by selecting the longest reads (Table S1). This subset was assembled using multiple
113 assembly tools dedicated to processing this large amount of data (Redbean[16],
114 SMARTdenovo[17] and Flye[18]). SMARTdenovo is not among the fastest algorithms and
115 has not been updated for several years, but since it can be easily parallelized, it remains an
116 interesting choice for assembling large genomes. The overlap and consensus calculations
117 were split into 60 chunks and each were run on a 32-core server and took about two days
118 and ten hours respectively. In comparison, Redbean was able to generate an assembly after
119 just seven days on a 64-core server with 3TB of memory while Flye needed 43 days on the
120 same computer server. Surprisingly, the redbean assembly had a cumulative size two times
121 higher than the expected genome size (29.6Gb vs 14.5Gb), a low contiguity and contained a
122 large amount of short contigs. The SMARTdenovo and Flye assemblies were highly
123 comparable, but Flye was the most contiguous (contigs N50 of 1.8 Mb vs 1.1 Mb) and
124 SMARTdenovo had a cumulative size closer to the expected one (14.1 Gb vs 13.0 Gb, Table
125 S3). Additionally, even though the assemblies were polished later, the raw SMARTdenovo
126 assembly contained a higher number of complete BUSCO genes (83.0% vs 49.5%) which
127 indicates that its consensus module is more efficient.

128 The SMARTdenovo and Flye assemblies were successively polished using Racon[19] and
129 Medaka (<https://github.com/nanoporetech/medaka>) with long reads and Hapo-G[20] with
130 short reads. Polished contigs were validated and organized into scaffolds using the DLE-1
131 optical map and proprietary tools provided by BNG. As expected, due to its lower cumulative

132 size, Flye scaffolds contained a larger proportion of unknown bases (851 Mb and 262 Mb).
133 Based on these results (proportion of gaps and gene completion), the assembly produced by
134 SMARTdenovo[17] was selected (Table S4). Local contig duplications (negative gaps) were
135 resolved using BiSCoT²², which improved the contigs N50 from 1.2 Mb up to 2.1 Mb. Finally,
136 the resulting assembly was polished one last time using Hapo-G[20] with short reads. This
137 led to 2,904 scaffolds (larger than 30kb) representing 14.26 Gb with a N50 of 48 Mb (79
138 scaffolds) and a maximum scaffold size of 254 Mb. Thus, the genome size is in the same
139 range as all other available reference quality assemblies of *T. aestivum*: e.g. 14.29 Gb for
140 cv. LongReach Lancer, 14.55 Gb for cv. Chinese Spring, and 14.96 Gb for cv. SY Mattis.

141 **Construction and validation of pseudomolecules**

142 We then guided the construction of the 21 chromosome sequences (i.e. pseudomolecules)
143 based on collinearity with the CS (Chinese Spring) RefSeq Assembly v2.1[22]. Given the
144 complexity of this hexaploid genome, we established a dedicated approach in order to
145 anchor each Renan scaffold based on similarity search against CS. To avoid problems due
146 to multiple mappings, we selected a dataset of uniquely mappable sequences. Genes are
147 not uniquely mappable since most of them are repeated as three homoeologous copies
148 sharing on average 97% nucleotide identity. In addition, the gene density (1 gene every
149 130kb on average) is too low to anchor small Renan scaffolds that do not carry genes. Thus,
150 we used 150 bp tags corresponding to the 5' and 3' junctions between a transposable
151 element (TE) and its insertion site (75 bps on each side) which are called ISBP (Insertion
152 Site-Based Polymorphism) markers and are highly abundant and uniquely mappable in the
153 wheat genome[23]. We designed a dataset of 5.76 million ISBPs from CS assembly which
154 represent 1 ISBP every 2.5kb. Their mapping enabled the anchoring of 2,566 scaffolds on
155 21 pseudomolecules representing 14.20 Gb (99% of the assembly). We then used Hi-C data
156 to validate the assembly and to correct the mis-ordered and mis-oriented scaffolds. The Hi-C
157 map revealed only a few inconsistencies, demonstrating that the collinearity between CS
158 and Renan was strong enough to guide the anchoring in a very accurate manner. The Hi-C
159 map-based curation led to the detection of 18 chimeric scaffolds that were split into 2 or 3
160 pieces and to the correction of the location and/or orientation of 198 scaffolds. The final
161 assembly was composed of 21 pseudomolecules (Figure 1) with 338 unanchored scaffolds
162 representing 61 Mb only.

163 **Quality assessment of the assembly**

164 First, we calculated the overall quality of the sequence using Merqury and Illumina reads.
165 We obtained an average quality value (QV) of 32.8, a lower QV than that obtained with

166 short-reads assemblies, but consistent with QV already reported for plant genomes
167 sequenced by ONT[24]. Indeed, using Illumina reads and the CS RefSeq v2.1 assembly,
168 Merqury computed a QV of 44.5 (Table 1). This shows that per-base quality is still an issue,
169 at least with the version of the technology used in this study. However, this could be
170 tempered by the fact that coding regions, due to lower repeating regions, may have higher
171 precision.

172 The completeness and quality of the assembly was estimated by searching for the presence
173 of known genes, i.e. the 107,891 High Confidence (HC) genes predicted in CS RefSeq v1.1.
174 We used BLAST[25] to search for the presence of each of the 461,476 exons larger than 30
175 bps in the Renan scaffolds, and we considered only matches showing at least 95% identity
176 over at least 95% query length. We found hits for 96.2% of the query exons with on average
177 99.3% identity, suggesting that the gene space is assembled at a high-quality level. The
178 missing genes/exons would correspond, in most of the cases, to real presence/absence
179 variations between CS and Renan while the nucleotide divergence between exons is 0.7%.
180 It was the first evidence that homoeologous gene copies, sharing on average 97%
181 identity[7], were not collapsed in the Renan assembly. We confirmed this by showing that
182 62% of the CS exons are strictly identical in Renan (and carried by the same chromosome).
183 Such level of nucleotide divergence between CS and Renan is similar to what has been
184 shown through whole genome alignments (Brinton et al. 2020).

185 We then assessed the assembly quality of the TE space by aligning the complete dataset of
186 ISBP markers of CS onto the Renan assembly. We found that 94% markers were conserved
187 (at least 90% identity over 90% query length) i.e., present in the assembly, revealing that the
188 TE space is extremely close to completeness. Indeed, 6% of missing markers is similar to
189 the proportion of expected Presence-Absence variations (PAVs) affecting TEs[26].

190 Additionally, we searched for telomeric repeats (TTTAGGG) in the 21 chromosomes and
191 found telomeric repeats at both ends of chromosome 7A, which is generally an indicator of
192 the completion of the chromosome sequence. Both ends of chromosome 7A were also
193 validated by the optical map (Figure S1).

194 **Impact of the polishing**

195 Based on BUSCO and the alignment of the IBSP markers from the CS assembly, we
196 monitored the evolution of the consensus quality through successive polishing iterations. As
197 previously described, the SMARTdenovo consensus allowed the recovery of a greater
198 number of complete BUSCO genes compared to that of Flye, which may be an indicator of
199 its greater accuracy. However, the BUSCO score was still low (83%) especially for a
200 hexaploid genome, underlining the importance of polishing raw assemblies. Likewise, we

201 were able to find 80.4% of the IBSP markers but only 7% were aligned without mismatch
202 between the two genotypes (Table S5). When polished with long-reads, the BUSCO score
203 reached 96.7% and 92.9% of the IBSP markers were retrieved (including 28.0% with perfect
204 matches). The subsequent polishing step with short reads weakly decreased the BUSCO
205 score (from 96.7% to 96.6%), but the proportion of duplicated genes increased from 83.1%
206 to 87.0% which is here wanted because in the case of a hexaploid genome most of the
207 genes are in three copies. Moreover, the proportion of perfectly aligned ISBP markers
208 drastically increased from 28.0% up to 58.9%. Although the polishing with short reads
209 weakly impacts the BUSCO conserved genes, the IBSP markers underline its importance in
210 the case of long reads assemblies. Since ISBPs are unique tags sampling the whole
211 genome, this analysis revealed that nucleotide errors were frequent before polishing,
212 affecting half of the sample loci. Thus, we showed that the polishing steps were successful,
213 even in this large and polyploid genome, and drastically improved the quality of the
214 consensus.

215 **Recent improvement of the ONT technology**

216 Oxford Nanopore Technology is evolving rapidly, and improvements to the base calling
217 softwares are frequent, allowing old data to be analyzed with the aim of improving read
218 accuracy and subsequent analysis. To measure the gain brought by each new version
219 during this project, we analyzed a subset of ultra-long reads (longer than 100kb) with
220 different basecallers or versions of the same basecaller: guppy 2.0, guppy 3.0.3 (High
221 Accuracy mode), guppy 3.6 (High Accuracy mode) and the recent bonito v0.3.1. We
222 observed a strong difference in accuracy, of around 7%, between guppy 2.0 and the newer
223 basecaller (bonito v0.3.1), representing the gain over the last two years (Figure S2A). This
224 significant improvement could lead nanopore users to reanalyze their old sequencing data to
225 improve the quality of their assemblies. As an example, the accuracy of raw nanopore reads
226 gained about 2% on average using guppy 3.6 (Table S6). We observed a reduction of the
227 number of contigs of 19%, and an improvement of the contig N50 of 26%. Likewise, the
228 cumulative size is slightly higher in the guppy 3.6 assembly, which may underline a smaller
229 amount of collapsed repetitive regions (Table S7).

230 More importantly, the identity percentage obtained when aligning ONT reads on the wheat
231 assembly is lower than what was obtained on yeast and human samples (Figure S2B). This
232 difference can be explained by the fact that, first, the consensus of the wheat genome is not
233 perfect and secondly, that basecallers are trained on a mixture which contains yeast and
234 human data. Indeed, DNA modification patterns can differ between taxa, and read accuracy
235 seems better when the model was trained on native DNA from the same species[27]. This

236 huge difference between the read accuracy of yeast and wheat samples should motivate
237 nanopore users to train basecaller models to their targeted species.

238 **Annotation of transposable elements and protein-coding genes**

239 We annotated TEs based on similarity search against our wheat-specific TE library
240 ClariTeRep[28] and raw results were then refined using CLARITE, a homemade program
241 able to resolve prediction conflicts, merge adjacent features into a single complete element,
242 and identify nested insertion patterns. We detected 3.9 million copies of TEs in the Renan
243 genome assembly, representing 12.0 Gb i.e. 84% of the assembly size. The proportions of
244 each superfamily were similar to what has been described for CS[29] (Table 2).
245 Gene annotation was achieved by, first, transferring genes predicted in CS RefSeq v2.1 by
246 homology using the MAGATT pipeline[22]. This allowed us to accurately transfer 105,243
247 (out of 106,801; 98%) HC genes and 155,021 (out of 159,846; 97%) Low Confidence genes.
248 Such a transfer of genes predicted in another genotype (here CS) avoided genome-wide *de*
249 *novo* gene prediction that may artificially lead to many differences between the annotations.
250 We thus focused *de novo* predictions using TriAnnot[30] only on the unannotated part of the
251 genome, representing 8.5% of the 14.2 Gb, after having masked transferred genes and
252 predicted TEs. For that purpose, we produced RNASeq data for Renan from 28 samples
253 corresponding to 14 different organs/conditions in replicates: grains at four developmental
254 stages (100, 250, 500, and 700 degree days) under heat stress and control conditions,
255 stems at two developmental stages, leaves at three stages, and roots at one stage),
256 representing on average 78.8 million read-pairs per sample i.e 2.2 billion read-pairs in total.
257 This method allowed us to predict 4,440 genes specific to Renan compared to CS i.e., 4% of
258 the gene complement. This is consistent with the extent of structural variations affecting
259 genomes of *Triticeae*[26]. Transfer of known genes, novel predictions, and manual curation
260 (limited to storage protein encoding genes), led us to annotate 109,552 protein-coding genes
261 on the Renan pseudomolecules.

262 **Comparison with existing hexaploid genome assemblies**

263 We compared our long-read assembly with 10 other available chromosome-scale
264 assemblies of wheat genomes. Although the gene content was similar between the different
265 assemblies, as expected, the assemblies based on short reads had a lower contiguity
266 (contig N50 values lower than 100kb compared to the 2 Mb of the assembly of the Renan
267 genome, Figure 2A-B). Logically, they also contained more gaps (around 40 times, Figure
268 2C). Interestingly, we found more gaps per Mb in the D subgenome compared to the A and
269 B subgenomes in Renan (Figure S3). This indicates that the D subgenome is more difficult

270 to assemble even though it has a smaller genome size and contains less repetitive
271 elements. The same trend was already observed in another polyploid genome, the rapeseed
272 and its two subgenomes A and C[11]. Chromosomes from the different assemblies had
273 similar length except for the *ArinaLrFor* and the SY_Mattis variety in which a translocation
274 has been previously described between chromosomes 5B and 7B[8] (Figure 2D).

275 In addition, we generated dotplots between CS and Renan homeologous chromosomes and
276 confirmed the strong collinearity between the two genomes (Figure 3). Whole chromosome
277 alignments highlighted 16 large-scale inversions (>5 Mb; up to 118 Mb) on 10 chromosomes
278 and 1 translocation of a ca. 45 Mb segment on chromosome 4A. We performed the same
279 comparisons with the 10 other available genomes of related varieties assembled at the
280 pseudomolecule level (Supplementary Data 1). It showed that only 2 of these inversions are
281 specific to Renan while the others are shared between several accessions. They correspond
282 to regions of 23 Mb on chr6B (position 398-421 Mb) and 10 Mb on chr7B (position 267-277
283 Mb).

284 **Haplotype characterisation**

285 Crop breeding involves the selection of desired traits and their combination to generate
286 improved genotypes. Generally, these traits correspond to genomic regions carrying genetic
287 variations or genes[31]. These regions of interest are inherited from their parents in the form
288 of large genomic blocks. The availability of several assemblies of the wheat genome now
289 allows the detection of these haplotypic blocks. Using the 11 chromosome-scale wheat
290 assemblies and an approach based on colored de Bruijn graphs, we investigated these
291 haplotypic blocks and applied our method to the 21 chromosomes of wheat. First, a colored
292 de Bruijn graph was built for each chromosome, where each colour represents a different
293 cultivar. Short (1kb) and evenly distributed (every 20kb) markers were extracted from each
294 chromosome and compared to the colored de Bruijn graph to extract their presence/absence
295 in each wheat cultivar. On each chromosome, the 15 most abundant presence/absence
296 profiles were selected and used to characterise haplotypic blocks. The haplotype blocks of
297 chromosome 6A, which is associated with productivity traits (as for example yield, grain size
298 and height), have already been expertized using a different method[31]. We obtained similar
299 results (Figure 4), except for the Chinese Spring chromosome 6A. Previous results have
300 assigned a unique haplotype to this wheat line. But in our case Chinese Spring exhibits the
301 same haplotype as SY Mattis, Jagger, Lancer and Norin61, which had previously been
302 described as sharing the same haplotype. These differences may be explained by the
303 stringency of the comparison, which perhaps should be adjusted separately for each
304 chromosome. Concerning the Renan cultivar, the chromosome 6A has haplotype blocks

305 similar to those of the ArinaLrFor line. Additionally, we used this method to investigate
306 haplotypic blocks that are specific to one or a subset of wheat cultivars.

307 **Identification of introgressions**

308 Introgression is an important source of genetic variation which is generally the signature of
309 breeding programmes, especially in wheat[32]. Several introgressions have already been
310 reported[8], notably in chromosomes 2B and 3D in LongReach Lancer and in chromosome
311 2A in Jagger, Mace, SY Mattis and CDC Stanley. Using our approach, we were able to
312 clearly identify the two introgressions in LongRead Lancer (Figure 5a), and the *Ae.*
313 *ventricosa* introgression in chromosome 2A (Figure 5b). In addition, we found that this
314 introgression of *Ae. ventricosa* is also present in the Renan cultivar (Figure 5b). The optical
315 map was aligned with this 34 Mb region of Renan and validated the correct structure of this
316 important region carrying multiple resistance genes (Yr17, Lr37, Sr38, Cre5). More
317 importantly, the 34 Mb consisted of 22 contigs in Renan and 2,339 in Jagger. A comparison
318 of the fragmentation near the introgression point is presented in Figure 5d and shows a large
319 difference between the long- and short-reads assemblies. Additionally, we also identified
320 several candidate introgressions, which had already been spotted through retrotransposon
321 profiles[8]: i) a 45-Mb region on chromosome 2D which is shared between the lines Julius,
322 ArinaLrFor, SY Mattis, Jagger and also Renan (Figure 6a); ii) a 53-Mb region at the end of
323 chromosome 3D in Lancer (Figure 6b); iii) a 48-Mb region at the beginning of chromosome
324 3D in SY Mattis (Figure 6b) and iv) the *Ae. ventricosa* introgression of 30-Mb in chromosome
325 7D which carries Pch1 resistance gene (Figures 6c).

326 Moreover, a known large-scale structural variation in chromosomes 5B and 7B of ArinaLrFor
327 and SY Mattis cultivars was also easily identifiable using haplotypic blocks of individual
328 chromosomes (Figure S4).

329 **Comparative analysis of a storage protein coding gene cluster in *T. aestivum***

330 Tandem duplications are an important mechanism in plant genome evolution and
331 adaptation[33,34] but the assembly of tandemly duplicated gene clusters is difficult,
332 especially with short reads. In order to illustrate the gain brought by this optimized assembly
333 process, we focused on an important locus on chromosome 1B known to carry multiple
334 copies of storage protein and disease resistance genes[35,36]. Among them, the genes
335 encoding omega-gliadins are not only duplicated in tandem, but are also composed of
336 microsatellite DNA in their coding part, making them particularly hard to assemble properly
337 from short reads. We compared orthologous regions harboring these genes between CS and
338 Renan, spanning 1.58 Mb and 2.32 Mb, respectively. The CS region was more fragmented

339 with 101 gaps versus only 3 in Renan (Figures 5a). The number of copies of omega-gliadin
340 encoding genes was quite similar: 9 in CS and 10 in Renan. The most striking difference
341 came from the completeness of the microsatellite motifs: 8 copies out of 9 contain N
342 stretches in CS RefSeq v2.1, revealing that the microsatellite is usually too large to be fully
343 assembled with short reads (Figure 5b). In contrast, all 10 copies predicted in Renan were
344 assembled completely. More generally, we mapped the corresponding proteins back to the
345 locus and showed that it was better reconstructed in the Renan assembly, with a mean
346 protein alignment length of 99% compared to 58% in CS (Figure 5c). In addition, the optical
347 map was used to validate the structure of this region in Renan and the assembly was
348 consistent with the three maps of this loci (Figure 5d).

349

350 **Comparative analysis of the locus that provides resistance to the orange** 351 **wheat blossom midge**

352 Like a few other wheat cultivars, Renan is resistant to the orange wheat blossom midge
353 (OWBM). The *Sm1* gene is known to confer resistance to wheat and a previous study has
354 shown that CDC Landmark is also resistant to the OWBM, and carries a 7.3-Mb haplotype
355 within the *Sm1* locus on chromosome 2B[8]. We extracted and aligned the corresponding
356 region of CDC Landmark on each cultivar, to precisely locate the corresponding region on
357 each chromosome 2B. From these eleven regions of 1-2 Mb, we computed the haplotypic
358 blocks using a higher resolution than previously (1 kb marker every 5 kb). This analysis
359 revealed a strong similarity of the *Sm1* locus between CDC Landmark and Renan (Figure
360 8a), the presence of the *Sm1* gene in blocks shared between the two cultivars. In addition, a
361 comparison of the fragmentation of these two regions underlines the higher contiguity of the
362 Renan assembly, with 4 contigs in the Renan *Sm1* locus compared to 62 in CDC Landmark
363 (Figure 8b). The *Sm1* locus of Renan is in agreement with the optical map and shows clearly
364 the three remaining gaps that may correspond to smaller and unanchored contigs.

365

366 **Discussion**

367 In this study, we showed that the recent improvement of the Oxford Nanopore Technology,
368 in terms of error rate and throughput, has opened up new perspectives in the age of long-
369 read technologies. Indeed, the sequencing and assembly of complex genomes, like the
370 hexaploid wheat, is now accessible to sequencing facilities. Additionally, the ability to
371 sequence ultra-long reads using ONT devices is a real advantage over the other long-read
372 technology, namely PACBIO. In this study, we were able to generate a coverage of 14X with
373 reads longer than 50kb, whereas PACBIO libraries, used to generate HiFi (High-Fidelity)
374 reads, are generally sized around 15kb[37,38]. Several studies have already underlined the

375 positive impact of these ONT ultra-long reads on the assembly contiguity[9,37,39]. In
376 contrast, the error rate that was previously a thorn in their side has been drastically reduced
377 over the last year. Herein we reported a quality score near Q10-Q15 for individual ONT
378 reads, as already shown[27], which is still far from what HiFi reads can provide, generally
379 near Q30[37]. The high accuracy of HiFi reads might be sufficient to distinguish copies from
380 repeat regions if they present few variations. The impact of ultra-long reads will lie mainly in
381 the case of identical repeats, and obviously, the presence of these particular cases will
382 depend on the evolutionary history of the studied genomes. In addition, this high error rate
383 has an impact on the consensus quality, and at the moment, a combination of ONT and
384 Illumina reads is still needed to achieve a decent per-base accuracy.

385

386 By following basecallers evolution, we noticed that the gain when using recent basecaller is
387 high and we guess this observation will encourage users to reprocess older data. However,
388 this is not trivial and it requires sufficient computing resources. Interestingly, we observed
389 that the error rate of ONT data is organism dependent and that the training of basecaller has
390 a significant impact on the overall quality of the reads[27]. This is, in our opinion, an
391 important fact because a large proportion of *de novo* assemblies now concern non-model
392 organisms and users will have to address this limitation of current software. There are
393 existing methods to train the basecaller on non-model species[40,41], but this can still be a
394 big barrier, depending on the size of the dataset, for many end users. However, as
395 highlighted in this study, the combination of long- and short-reads sequencing with polishing
396 methods greatly improves the consensus sequence of a given genome assembly and these
397 algorithms seem sufficient at least in coding regions.

398

399 Even though there are now several chromosome-scale assemblies of the hexaploid wheat
400 genome, this assembly of the Renan variety based on long-reads will benefit biologists and
401 geneticists as it offers a high resolution. We show that our chromosome-scale assembly of
402 Renan based on long reads can bring new insight into genomic regions of interest. In
403 particular, in regions that carry multiple resistance genes, as a large *Ae. ventricosa*
404 introgression shared with other cultivars on chromosome 2A and a unique *Ae. ventricosa*
405 introgression on chromosome 7D. The lower number of gaps in these regions will help to
406 localize genes of interest and to have a better understanding of the impact of these
407 introgressions. Additionally, we demonstrated by examining two important locus, containing
408 prolamin and resistance genes that such regions are truly enhanced and contain very few
409 gaps compared to assemblies based on short reads.

410

411 Moreover, unlike recent chromosome-scale assemblies, Renan's gene prediction is not only
412 a projection of Chinese Spring gene models, but also includes *de novo* annotation with RNA-
413 Seq data which is of real benefit for the construction of pan genome (or pan annotation) or
414 when cultivar-specific genes are examined. For all of these reasons, we believe this high
415 resolution assembly will benefit the wheat community and help breeding programs dedicated
416 to the bread wheat genome.

417

418 Methods

419 Plant material and DNA extraction

420 *Triticum aestivum* cv. Renan seeds were provided by the INRAE Biological Resource Center
421 on small grain cereals and grown for two weeks and a dark treatment was applied on the
422 seedlings for two days before collecting leaf tissues.

423 For the sequencing experiments, DNA was isolated from frozen leaves using QIAGEN
424 Genomic-tips 100/G kit (Cat No./ID: 10243) and following the tissue protocol extraction.
425 Briefly, 1g of leaves were ground in liquid nitrogen with mortar and pestle. After 3h of lysis
426 and one centrifugation step, the DNA was immobilized on the column. After several washing
427 steps, DNA is eluted from the column, then desalted and concentrated by alcohol
428 precipitation. The DNA is resuspended in the TE buffer.

429 To generate the optical map, uHMW DNA were purified from 0.5 gram of very young fresh
430 leaves according to the Bionano Prep Plant tissue DNA Isolation Base Protocol (30068 -
431 Bionano Genomics) with the following specifications and modifications. Briefly, the leaves
432 were fixed using a fixing solution (Bionano Genomics) containing formaldehyde (Sigma-
433 Aldrich) and then grinded in a homogenization buffer (Bionano Genomics) using a Tissue
434 Ruptor grinder (Qiagen). Nuclei were washed and embedded in agarose plugs. After
435 overnight proteinase K digestion in Lysis Buffer (Bionano Genomics) and one hour treatment
436 with RNAse A (Qiagen), plugs were washed four times in 1x Wash Buffer (Bionano
437 Genomics) and five times in 1x TE Buffer (ThermoFisher Scientific). Then, plugs were
438 melted two minutes at 70°C and solubilized with 2 µL of 0.5 U/µL AGARase enzyme
439 (ThermoFisher Scientific) for 45 minutes at 43°C. A dialysis step was performed in 1x TE
440 Buffer (ThermoFisher Scientific) for 45 minutes to purify DNA from any residues. The DNA
441 samples were quantified by using the Qubit dsDNA BR Assay (Invitrogen). Quality of
442 megabase size DNA was validated by pulsed field gel electrophoresis (PFGE).

443 **Illumina Sequencing**

444 DNA (1.5µg) was sonicated using a Covaris E220 sonicator (Covaris, Woburn, MA, USA).
445 Fragments (1µg) were end-repaired, 3'-adenylated and Illumina adapters (Bioo Scientific,
446 Austin, TX, USA) were then added using the Kapa Hyper Prep Kit (KapaBiosystems,
447 Wilmington, MA, USA). Ligation products were purified with AMPure XP beads (Beckman
448 Coulter Genomics, Danvers, MA, USA). Libraries were then quantified by qPCR using the
449 KAPA Library Quantification Kit for Illumina Libraries (KapaBiosystems), and library profiles
450 were assessed using a DNA High Sensitivity LabChip kit on an Agilent Bioanalyzer (Agilent
451 Technologies, Santa Clara, CA, USA). The library was sequenced on an Illumina NovaSeq
452 instrument (Illumina, San Diego, CA, USA) using 150 base-length read chemistry in a
453 paired-end mode. After the Illumina sequencing, an in-house quality control process was
454 applied to the reads that passed the Illumina quality filters[42]. These trimming and removal
455 steps were achieved using Fastxtend tools (<https://www.genoscope.cns.fr/fastxtend/>).

456 **Nanopore Sequencing**

457 Libraries were prepared according to the protocol Genomic DNA by ligation (SQK-LSK109
458 kit). Genomic DNA fragments (1.5 µg) were repaired and 3'-adenylated with the NEBNext
459 FFPE DNA Repair Mix and the NEBNext® Ultra™ II End Repair/dA-Tailing Module (New
460 England Biolabs, Ipswich, MA, USA). Sequencing adapters provided by Oxford Nanopore
461 Technologies (Oxford Nanopore Technologies Ltd, Oxford, UK) were then ligated using the
462 NEBNext Quick Ligation Module (NEB). After purification with AMPure XP beads (Beckmann
463 Coulter, Brea, CA, USA), the library was mixed with the Sequencing Buffer (ONT) and the
464 Loading Bead (ONT) and loaded on MinION or PromethION R9.4.1 flow cells. One
465 PromethION run was performed with Genomic DNA purified with Short Read Eliminator kit
466 (Circulomics, Baltimore, MD, USA) before the library preparation.

467 **Optical Maps**

468 Labeling and staining of the uHMW DNA were performed according to the Bionano Prep
469 Direct Label and Stain (DLS) protocol (30206 - Bionano Genomics). Briefly, labeling was
470 performed by incubating 750 ng genomic DNA with 1× DLE-1 Enzyme (Bionano Genomics)
471 for 2 hours in the presence of 1× DL-Green (Bionano Genomics) and 1× DLE-1 Buffer
472 (Bionano Genomics). Following proteinase K digestion and DL-Green cleanup, the DNA
473 backbone was stained by mixing the labeled DNA with DNA Stain solution (Bionano
474 Genomics) in presence of 1× Flow Buffer (Bionano Genomics) and 1× DTT (Bionano
475 Genomics), and incubating overnight at room temperature. The DLS DNA concentration was
476 measured with the Qubit dsDNA HS Assay (Invitrogen).

477 Labelled and stained DNA was loaded on Saphyr chips. Loading of the chips and running of
478 the Bionano Genomics Saphyr System were all performed according to the Saphyr System
479 User Guide (30247 - Bionano Genomics). Data processing was performed using the
480 Bionano Genomics Access software.

481 A total of 4541 Gb data were generated. From this data, molecules with a size larger than
482 150kb were filtered generating 1931 Gb of data. These filtered data, corresponding to 128x
483 coverage of the *Triticum aestivum* cv. Renan consists of 7,810,298 molecules with an N50 of
484 237.5kb and an average label density of 14.3/100kb. The filtered molecules were aligned
485 using RefAligner with default parameters. It produced 1053 genome maps with a N50 of 37.5
486 Mbp for a total genome map length of 14946.8 Mbp.

487 **RNA extraction**

488 Several tissues (stem, leaves, root or grain) were collected on plants with different growth
489 conditions and of different ages. Each of these 28 tissues was subjected to RNA extraction
490 with the following protocole: 200mg to 1g of fine powder was put in a 50ml falcon tube with
491 4.5 ml of NTES buffer [0.1 M NaCl, 1% SDS, 10 mM Tris-HCl (pH 7.4), 1 mM EDTA(pH 8)].
492 After vortexing the tube, 3ml of phenol-chloroforme-IAA were added. The tube was mixed for
493 10 minutes and centrifuged for 20 minutes at 5,000 rpm (15°C). The aqueous phase was
494 collected and placed in a new 15ml tube. 3ml of phenol-chloroforme-IAA were added. The
495 tube was mixed for 10 minutes and centrifuged for 20 minutes at 5,000 rpm (15°C). The
496 aqueous phase was collected and placed in a new 50ml tube. 1/10 of AcNa 3M (pH 5.2)
497 and 2 volumes of 100% ethanol were added. The tube was mixed gently by turning and
498 centrifuged 20 minutes at 5,000 rpm (4°C). The supernatant was removed. The precipitate
499 was dried and resuspended in 20 µl RNase free water. A treatment with DNase was
500 realized and the RNA were purified on a MinElute column (Qiagen). A second treatment with
501 DNase was realized by adding DNase directly on the filter. After ethanol cleanup, the
502 column was eluted with 14 µl of RNase free water. The quality of the RNA was evaluated
503 using RNA 6000 Nano Assay chip for size and RIN estimation and spectrophotometry
504 (A260/A280 and A260/A230 ratios) for purity estimation. The RNA were quantified using
505 Qubit RNA high sensitivity Assay kit (Invitrogen).

506 **RNA sequencing**

507 RNA-Seq library preparations were carried out from 500ng to 2000ng of total RNA using the
508 TruSeq Stranded mRNA kit (Illumina, San Diego, CA, USA), which allows mRNA strand
509 orientation (sequence reads occur in the same orientation as antisense RNA). Briefly,
510 poly(A)+ RNA was selected with oligo(dT) beads, chemically fragmented and converted into

511 single-stranded cDNA using random hexamer priming. Then, the second strand was
512 generated to create double-stranded cDNA. cDNA were then 3'-adenylated, and Illumina
513 adapters were added. Ligation products were PCR-amplified. Ready-to-sequence Illumina
514 libraries were then quantified by qPCR using the KAPA Library Quantification Kit for Illumina
515 Libraries (KapaBiosystems, Wilmington, MA, USA), and libraries profiles evaluated with an
516 Agilent 2100 Bioanalyzer (Agilent Technologies, Santa Clara, CA, USA). Each library was
517 sequenced using 151 bp paired end reads chemistry on an Illumina NovaSeq 6000
518 sequencer (Illumina, San Diego, CA, USA).

519 **Long reads genome assembly**

520 The 20 ONT runs were basecalled using two versions of guppy: 3.3 HAC and 3.6 HAC
521 (Table S6). We monitored the gain of each guppy basecaller release and evaluated three
522 different assemblers in the context of large genomes: Redbean[16] v2.5 (git commit
523 3d51d7e), SMARTdenovo[17] (git commit 5cc1356) and Flye[18] v2.7 (git commit 5c12b69).
524 All assemblers were launched using a subset of reads consisting of 30X of the longest reads
525 (Table S3). Then, we selected one of the assemblies based not only on contiguity metrics
526 such as N50 but also cumulative size, proportion of unknown bases. The Flye (longest
527 reads) and SMARTdenovo (all reads) assemblies were very similar in terms of contiguity but
528 we decided to keep the SMARTdenovo assembly as its cumulative size was higher. The
529 SMARTdenovo assembler using the longest reads resulted in a contig N50 of 1.1Mb and a
530 cumulative size of 14.07Gb. As nanopore reads contain systematic error in homopolymeric
531 regions, we polished the consensus of the selected assembly with nanopore reads as input
532 to the Racon (v1.3.2, git commit 5e2ecb7) and Medaka softwares. In addition, we polished
533 the assembly two additional times using Illumina reads as input to the Hapo-G tool (v1.0, git
534 commit).

535 **Long range genome assembly**

536 The Bionano Genomics scaffolding workflow (Bionano Solve version 3.5.1) was launched
537 with the nanopore contigs and the Bionano map. We found in several cases that the
538 nanopore contigs were overlapping (based on the optical map) and these overlaps were
539 corrected using the BiSCoT software[21] with default parameters. Finally, the consensus
540 sequence was polished once more using Hapo-G and short reads, to ensure correction of
541 duplicate regions that were collapsed (Table S4).

542 **Validation of the *Triticum aestivum* cv Renan assembly**

543 The quality value (QV) of the Renan and CS assemblies was obtained using Merqury[43].
544 First, 31-mers were extracted from the Renan and CS Illumina sequencing reads
545 (accessions SRR5893651, SRR5893652, SRR5893653 and SRR5893654) and then the QV
546 of each genome assembly was computed using Merqury (version 1.3, git commit 6b5405e).
547 We used BLAST[25] to search for the presence of 107,891 HC genes from CS RefSeq v1.1
548 in the Renan genome sequence. We extracted the 461,476 individual exons larger than 30
549 bps and without Ns from this dataset and computed exon-by-exon BLAST in order to avoid
550 spurious sliced alignments. An exon was considered present if it matched the Renan
551 scaffolds with at least 95% identity over at least 95% of its length. To estimate the proportion
552 of identical exons between CS and Renan and the average nucleotide identity, we used the
553 same BLAST-based procedure but while restricting the dataset to 454,008 CS exons that
554 are on pseudomolecules (excluding chrUn) and considering Renan pseudomolecules
555 instead of scaffolds i.e., only exons carried by the same chromosome in CS and Renan were
556 considered. We extracted all available ISBPs (150 bps each) from the CS RefSeq v1.1 and
557 filtered out ISBPs containing Ns and those that do not map uniquely on the CS genome. This
558 led to the design of a dataset containing 5,394,172 ISBPs which were aligned on the Renan
559 scaffolds using BLAST. We considered an ISBP was conserved in Renan if it matched with
560 at least 90% identity over 90% of its length. We used the same ISBP dataset to study the
561 impact of polishing on error rate in the assembly while using BLAST and considering at least
562 90% identity over at least 145 aligned nucleotides.

563 **Anchoring of the *Triticum aestivum* cv Renan assembly**

564 We guided the construction of 21 Renan pseudomolecules based on collinearity with the CS
565 RefSeq Assembly v2.1. For this, we used the positions of conserved ISBPs as anchors
566 (5,087,711 ISBPs matching with $\geq 80\%$ identity over $\geq 90\%$ query overlap). This
567 represented 357 ISBPs/Mb, meaning that even the smallest scaffolds (30kb) carried
568 generally more than 10 potential anchors. However, some ISBPs match at non-orthologous
569 positions which create noise to precisely determine the order and orientation of some
570 scaffolds. To overcome this issue, we considered ISBPs by pairs. Only pairs of adjacent
571 ISBPs (i.e. separated by less than 50kb on both CS and Renan genomes) were kept as valid
572 anchors, allowing the filtering out of isolated mis-mapped ISBPs. Only scaffolds harboring at
573 least 50% of valid ISBP pairs on a single chromosome were kept. The others were
574 considered unanchored and they comprised the "chrUn". We calculated the median position
575 of matching ISBP pairs along each CS chromosome for defining the order of the Renan
576 scaffolds relative to each other. Their orientation was retrieved from the orientation of all

577 matching ISBP pairs in CS following the majority rule. We thus built 21 pseudomolecules
578 that were then corrected according to the HiC map as explained hereafter.
579 Two Hi-C biological replicates were prepared from ten-days plantlets of *Triticum aestivum*
580 cv. Renan following the Arima Hi-C protocol (Arima Hi-C User Guide for Plant Tissues DOC
581 A160106 v01). For each replicate, two libraries were constructed using the Kapa Hyper Prep
582 kit (Roche) according to Arima's recommendation (Library Preparation using KAPA Hyper
583 Prep Kit DOC A160108 v01). The technical replicates were then pooled and sent to Genewiz
584 for sequencing on an Illumina HiSeq4000 (four lanes in total), reaching a 35x coverage. We
585 mapped a sample of 240 million read pairs with BWA-MEM (Burrows-Wheeler Aligner, Heng
586 Li, 2013) to the formerly built 21 pseudomolecules, filtered out for low quality, sorted, and
587 deduplicated using the Juicer pipeline[44]. We produced a Hi-C map from the Juicer output
588 by the candidate assembly visualizer mode of 3D-DNA pipeline[45] and visualized it with the
589 Juicebox Assembly Tools software. Based on abnormal frequency contacts signals revealing
590 a lack of contiguity, scaffold-level modifications of order, orientation and/or chimeric scaffolds
591 were identified in order to improve the assembly. In case of chimeric scaffolds, coordinates
592 of resulting fragments were retrieved from the Juicebox Assembly Tools application but then
593 recalculated to correspond precisely to the closest gap in the scaffold. Pseudomolecules
594 were eventually rebuilt from initial scaffolds and new fragments while adding 100N gaps
595 between neighbor scaffolds. A final Hi-C map was built to validate the accuracy of the final
596 assembly.

597 **Calculation of chromosome coverage**

598 Short (*Triticum aestivum* cv Renan and *Ae. ventricosa*) and long-reads (*Triticum aestivum* cv
599 Renan) were aligned using minimap2 (with the following parameters '-l 17G -2 --sam-hit-only
600 -a -x sr' and '-l 17G -2 --sam-hit-only --secondary=no -a -x map-ont' respectively).
601 Coverage of individual chromosomes was calculated in 1 Mb windows using mosdepth[46]
602 (version 0.3.1) and the following parameters '--by 1000000 -n -i 2 -Q 10 -m'. Note that the '-i
603 2' and '-Q 10' parameters were used to keep only alignments of reads that mapped in a
604 proper pair and with a minimal quality value of 10. Coverage of individual chromosomes was
605 plotted in Figure 1. In addition, large deletions and duplications were detected using
606 CNVnator[47] with the Illumina bam file and a window of 100bp. We focused on large events
607 (>500kb) and detected only 15 deletions and no duplication (Figure 1).

608 **Transposable elements annotation**

609 Transposable elements were annotated using CLARITE[28]. Briefly, TEs were identified
610 through a similarity search approach based on the ClariTeRep curated databank of repeated

611 elements using RepeatMasker (www.repeatmasker.org) and modelled with the CLARITE
612 program that was developed to resolve overlapping predictions, merge adjacent fragments
613 into a single element when necessary, and identify patterns of nested insertions[28].

614 **Gene prediction**

615 We used MAGATT pipeline (Marker Assisted Gene Annotation Transfer for Triticeae,
616 <https://forgemia.inra.fr/umr-gdec/magatt>) to map the full set of 106,801 High Confidence and
617 159,848 Low Confidence genes predicted in Chinese Spring IWGSC RefSeq v2.1. The
618 workflow implemented in this pipeline was described in Zhu et al.[22]. Briefly, it uses gene
619 flanking ISBP markers in order to determine an interval that is predicted to contain the gene
620 before homology-based annotation transfer, limiting problems due to multiple mapping.
621 When the interval is identified, MAGATT uses BLAT[48] to align the gene (UTRs, exons, and
622 introns) sequence and recalculate all sub-features coordinates if the alignment is full-length
623 and without indels. If the alignment is partial or contains indels, it runs GMAP[49] to perform
624 spliced alignment of the candidate CDS inside the interval. If no ISBP-flanked interval was
625 determined or if both BLAT and GMAP failed to transfer the gene, MAGATT runs GMAP
626 against the whole genome, including the unanchored fraction of the Renan assembly. We
627 kept the best hit considering a minimum identity of 70% and a minimum coverage of 70%,
628 with *cross_species* parameter enabled.

629 We then masked the genome sequence based on mapped genes and predicted
630 transposable elements coordinates using BEDTools[50] mergeBed and maskfasta v2.27.1.
631 Hence, we computed a *de novo* gene prediction on the unannotated part of the genome. We
632 used TriAnnot[30] to call genes based on a combination of evidence: RNA-Seq data, *de*
633 *novo* predictions of gene finders (FGeneSH, Augustus), similarity with known proteins in
634 *Poaceae*, as described previously[7]. For that purpose, we mapped RNA-Seq reads with
635 hisat2[51] v2.0.5, called 277,505 transcripts with StringTie[52] v2.0.3, extracted their
636 sequences with Cufflink[53] gffread v2.2.1, and provided this resource as input to TriAnnot.
637 We optimized TriAnnot workflow to ensure a flawless use on a cloud-based hpc cluster (10
638 nodes with 32 CPUs/128GB RAM each and shared file system) using the IaaS Openstack
639 infrastructure from the UCA Mesocentre. Gene models were then filtered as follows: we
640 discarded gene models that shared strong identity ($\geq 92\%$ identity, $\geq 95\%$ query coverage)
641 with an unannotated region of the Chinese Spring RefSeq v2.1, considered as doubtful
642 predictions. We then kept all predictions that matched RNASeq-derived transcripts ($\geq 99\%$
643 identity, $\geq 70\%$ query and subject coverage). For those that did not show evidence of
644 transcription, we kept gene models sharing protein similarity ($\geq 40\%$ identity, $\geq 50\%$ query

645 and subject coverage) with a *Poaceae* protein having a putative function (filtering out based
646 on terms "unknown", "uncharacterized", and "predicted protein").

647 **Comparison of genome assemblies**

648 Genome assemblies were downloaded from <https://webblast.ipk-gatersleben.de/downloads>.
649 Contigs were extracted by splitting input sequences at each N and standard metrics were
650 computed. Gene completion metrics were calculated using BUSCO v5.0 and version 10 of
651 the poales geneset which contains 4896 genes.

652 We built dotplots between Renan, CS and 10 other reference quality genomes (*ArinaLrFor*,
653 CDC Landmark, CDC Stanley, Jagger, Julius, LongReach Lancer, Mace, Norin61, SY
654 Mattis, spelta PI190962) by using orthologous positions of conserved ISBPs (1 ISBP every
655 2.5kb on average) identified by mapping them with BWA-MEM (maximum 2 mismatches,
656 100% coverage and minimal mapping quality of 30).

657 **Characterisation of haplotypic blocks**

658 First a colored de Bruijn graph was built for each chromosome from the eleven available
659 chromosome-scale assemblies of wheat (Renan, CS, *ArinaLrFor*, CDC Landmark, CDC
660 Stanley, Jagger, Julius, LongReach Lancer, Mace, Norin61 and SY Mattis). The colored de
661 Bruijn graph was created using Bifrost[54] with 31-mers and a unique color for each wheat
662 cultivar. In a second step, we extracted short markers (1kb) evenly spaced (20kb or 5kb) on
663 each chromosome and queried the colored de Bruijn graph using Bifrost and the following
664 parameter '-e 0.95' (for the comparison of each chromosome) and '-e 0.97' (for the
665 comparison of the *Sm1* locus). This parameter is the ratio of k-mers from queries that must
666 occur in the graph to be reported as present. For whole chromosome analyses, the 20kb
667 blocks were merged into 1-Mb blocks (the most abundant colour in the 50 20kb blocks was
668 retained for the 1Mb block). Individual blocks and *Ae. ventricosa* coverage were displayed
669 using RIdeogram[55].

670 **Comparison of a storage protein coding gene cluster**

671 We performed manual curation of the gene models encoding storage proteins predicted in
672 Renan. Protein sequences of prolamin and resistance genes[35] from a 1B chromosome
673 locus were downloaded and aligned to the CS and Renan genomes using BLAT[48] with
674 default parameters. Draft alignments were refined by aligning the given protein sequence
675 and the genomic region defined by the blat alignment using Genewise with default
676 parameters. Resulting alignments were filtered in order to conserve only the best match for
677 each position by keeping only the highest-scoring alignment and the genomic region

678 containing the gene cluster was extracted. Then, we used the jcv suite[56] with the mcscan
679 pipeline to find synteny blocks between both genomes. First, we used the
680 “jcv.compara.catalog” command to find orthologs and then the “jcv.compara.synteny
681 mcscan” with “--iter=1” command to extract synteny blocks. Finally, we generated the figure
682 with the “jcv.graphics.synteny” command and manually edited the generated svg file to
683 improve the quality of the resulting image by changing gene colors, incorporating gaps and
684 renaming genes. Moreover, to make the figure clearer, we artificially reduced the intergenic
685 space by 95% so that gene structures appear bigger. The omega gene cluster
686 representation figure was generated by using DnaFeaturesViewer[57] with coordinates of
687 features generated by the mcscan pipeline used previously.

688

689 Additional files

690 All the supporting data are included in two additional files: (a) A supplementary file which
691 contains Supplementary Tables 1-7 and Supplementary Figures 1-3; (b) A supplementary
692 file which contains dotplots of the 21 chromosomes of Renan with other wheat genome
693 assemblies.

694

695 Acknowledgements

696 This work was supported by the Genoscope, the Commissariat à l'Énergie Atomique et aux
697 Énergies Alternatives (CEA) and France Génomique (ANR-10-INBS-09-08). The biological
698 material (i.e. plant production, sample management, DNA and RNA extractions performed
699 by Caroline Pont and Cécile Huneau at GDEC) have been obtained in the framework of the
700 France Génomique WheatOMICS project (2017-2021) coordinated by Jérôme Salse. The
701 authors are grateful to Oxford Nanopore Technologies Ltd for providing early access to the
702 PromethION device through the PEAP, and we thank the staff of Oxford Nanopore
703 Technologies Ltd for technical help. We are grateful to the Mésocentre Clermont Auvergne
704 University and/or AuBi platform for providing help and/or computing and/or storage
705 resources.

706 Availability of supporting data

707 The Illumina and PromethION sequencing data and the Bionano optical map are available in
708 the European Nucleotide Archive under the following project PRJEB49351. The genome
709 assembly and gene predictions are freely available from the Genoscope website
710 <http://www.genoscope.cns.fr/plants/>.

711 Additionally, all the data and scripts used to produce the main figures are available on a
712 github repository <https://github.com/institut-de-genomique/Renan-associated-data>

713 Competing interests

714 The authors declare that they have no competing interests. JMA received travel and
715 accommodation expenses to speak at Oxford Nanopore Technologies conferences. JMA
716 and CB received accommodation expenses to speak at Bionano Genomics user meetings.

717 Funding

718 This work was supported by the Genoscope, the Commissariat à l'Énergie Atomique et aux
719 Énergies Alternatives (CEA) and France Génomique (ANR-10-INBS-09-08). CM postdoc
720 was funded by the SRESRI/Région Auvergne-Rhône-Alpes.

721 Author's contributions

722 SA, ID and AB extracted the sequenced DNA and generated the optical map. KL and AA
723 optimized and performed the nanopore and Illumina sequencing. NP, EP and MR generated
724 the Hi-C libraries and sequences. JMA, SE, BI, CM, PLZ, CB, HR, PL, DG and FC
725 performed the bioinformatic analyses. JMA, SE, BI, CM, PLZ, CB, CC, HR, PL and FC wrote
726 the article. JMA, PW and FC supervised the study.

727 **Table 1:** Comparison of *Triticum aestivum* L. genome assemblies. *NG50 and NG90 were
728 calculated using a genome size of 15Gb.

		Renan This study	Chinese Spring RefSeq_v2.1 from Zhu et al.[22]
Number of contigs		12,982	306,746
Cumulative size (bp)		14,001,122,256	14,317,423,665
N50 (bp)		2,159,703	341,062
L50		1,958	12,223
N90 (bp)		598,285	32,302
L90		6,645	59,261
NG50* (bp)		1,973,000	322,161
LG50		2,202	13,254
NG90* (bp)		264,272	16,550
LG90		8,816	85,688
Longest contig (bp)		15,116,687	3,528,546
Number of chromosomes		21	21
Cumulative size (bp)		14,195,643,615	14,225,829,371
N50 (bp)		703,299,328	713,360,512
L50		10	10
N90 (bp)		520,815,552	518,332,608
L90		19	19
Longest (bp)		854,463,248	851,934,019
% of N		1.78%	1.52%
BUSCO on assemblies (N=4,896)	Complete	99.1%	99.3%
	Duplicated	94.7%	96.1%
	Fragmented	0.1%	0.1%
	Missing	0.8%	0.6%
Base accuray - Quality Value (kmer)		32.8	44.5
Number of genes		109,552	107,891
Average number of exons		5.10	5.33
BUSCO on gene predictions (N=4,896)	Complete	99.1%	99.5%
	Duplicated	94.6%	98.2%
	Fragmented	0.2%	0.1%
	Missing	0.7%	0.4%

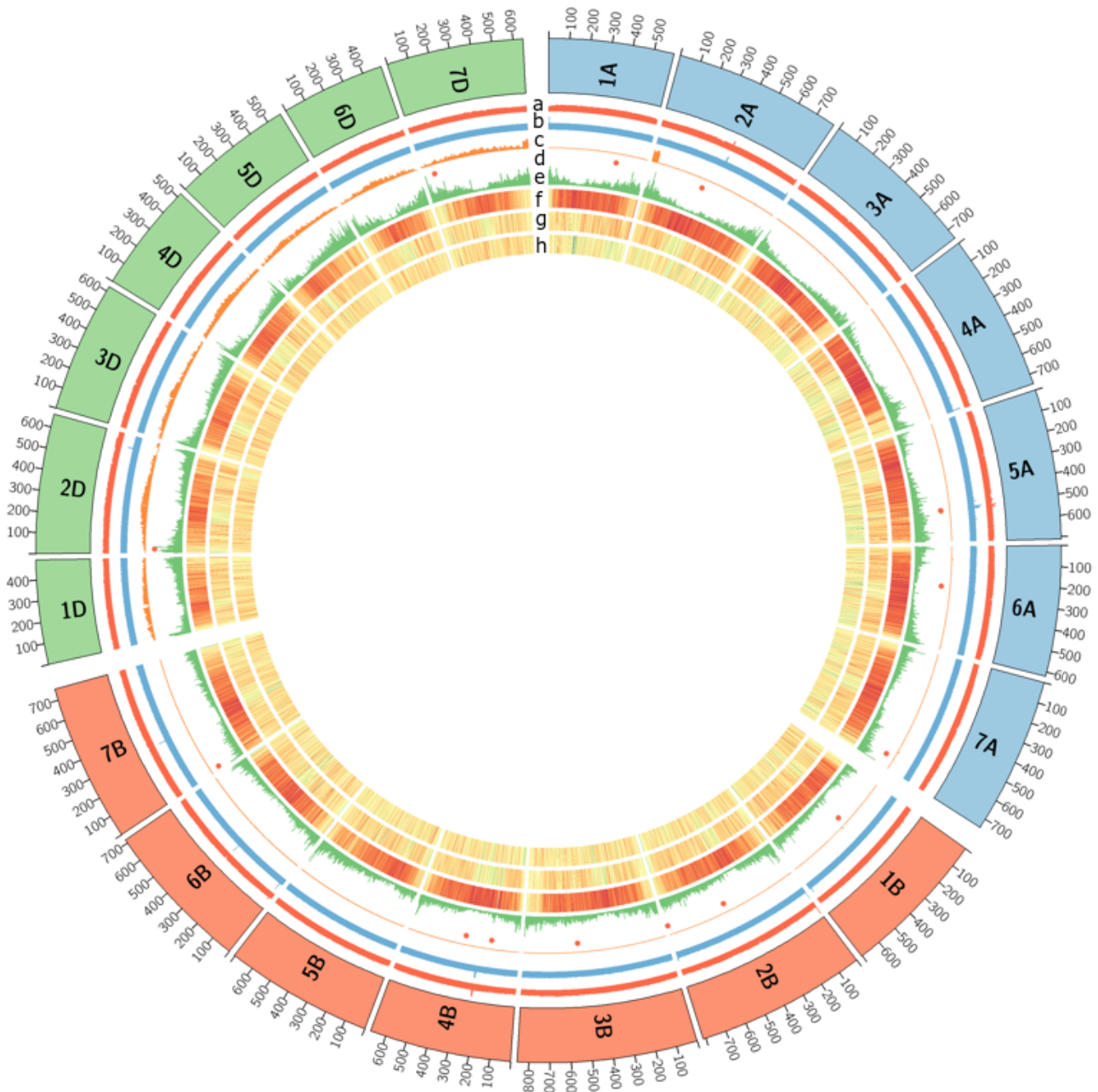
729 **Table 2:** TE classes proportions in Chinese Spring and Renan genome assemblies.

730

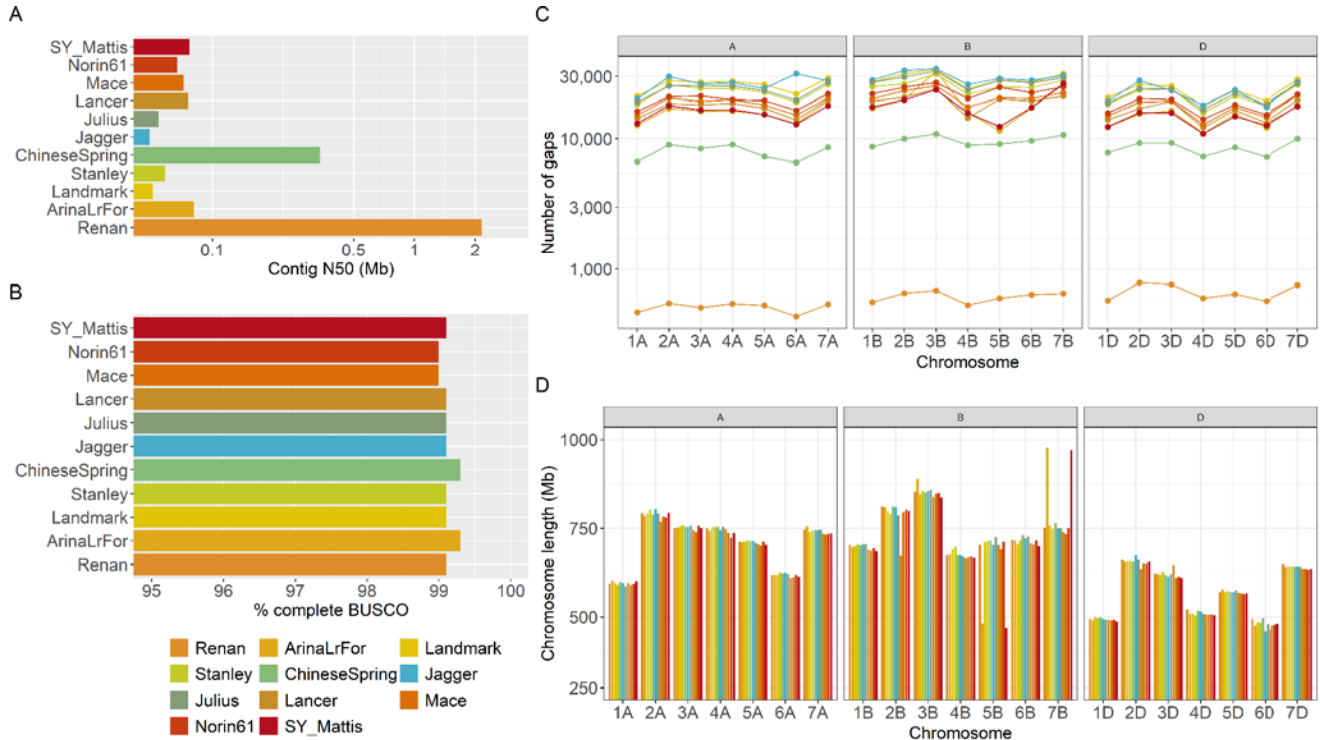
	Chinese Spring RefSeq_v1.0 from Zhu et al. [22]	Chinese Spring RefSeq_v2.1 from Zhu et al.[22]	Renan RefSeq_v2.0
Genome size (bp)	14,066,280,851	14,225,829,371	14,195,643,615
TE (bp)	11,921,309,743	12,092,094,168	11,967,447,100
TE (%)	84.7	85.0	84.3
Class I (Retrotransposons)	67.6	66.9	66.6
Gypsy (RLG)	46.7	46.1	45.8
Copia (RLC)	16.7	16.5	16.5
Unclassified LTR retrotransposons (RLX)	3.24	3.3	3.2
LINE (RIX)	0.9	1.1	1.1
SINE (SIX)	0.01	0.01	0.01
Class II (DNA transposons)- Subclass 1	16.5	17.0	16.9
CACTA (DTC)	15.5	15.9	15.8
Mutator (DTM)	0.38	0.44	0.44
Unclassified DNA transposons with TIR (DTX)	0.21	0.24	0.24
Harbinger (DTH)	0.16	0.18	0.18
Mariner (DTT)	0.16	0.17	0.17
Unclassified DNA transposons (DXX)	0.06	0.06	0.06
hAT (DTA)	0.006	0.009	0.009
Helitrons (DHH)	0.004	0.01	0.01
Unclassified TE (XXX)	0.68	0.95	0.82

731

732 **Figure 1.** Genome overview of the 21 chromosomes of hexaploid *T. aestivum* Renan (the 7
733 A chromosomes are in blue, the 7 B chromosomes in orange and the 7 D chromosomes in
734 green). From inner to outer track: (a) Coverage with short reads, (b) Coverage with long
735 reads, (c) coverage with *Ae. ventricosa* short reads, (d) Red dots represent large deletions
736 (>500Kb), (e) Gene density, (f) Density of CACTA (DNA transposon) elements, (g) Density
737 of Copia elements, (h) Density of Gypsy elements. All densities and coverage are calculated
738 in 1-Mb windows; yellow and red colors in density plots indicate lower and higher values,
739 respectively.



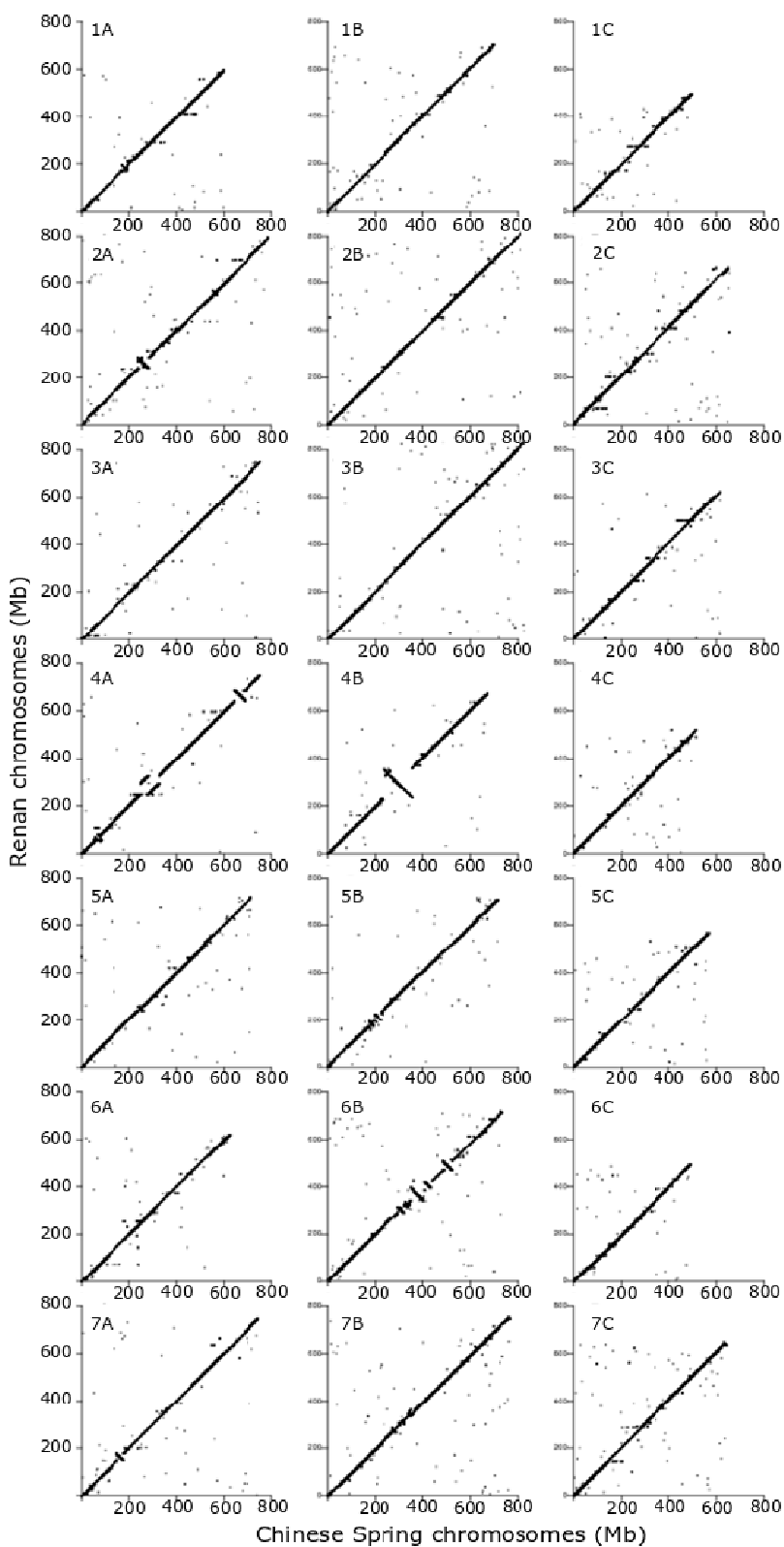
741 **Figure 2.** Comparison of existing hexaploid genome assemblies **A.** contig N50 values in
 742 Mbp. **B.** Proportion of complete BUSCO genes found in each assembly (N=4,896). **C.**
 743 Number of gaps in each chromosome. **D.** chromosome length in Mb.



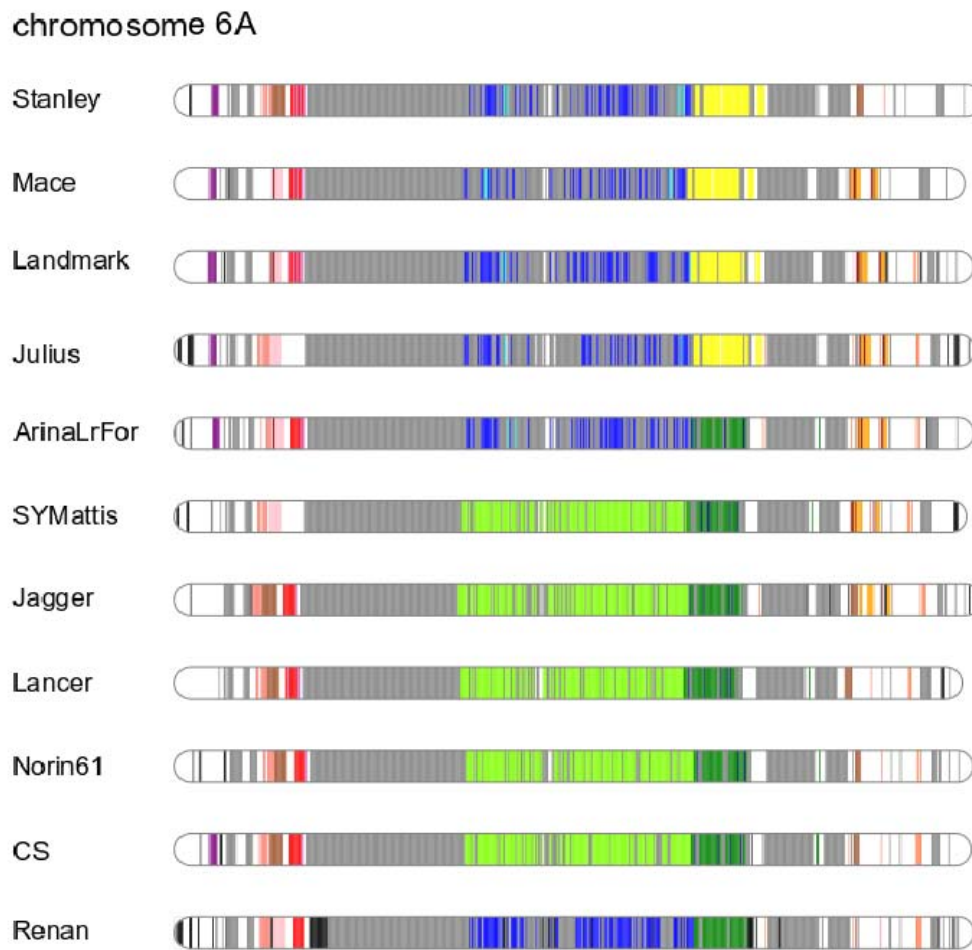
744

745 **Figure 3.** Dotplot comparisons of the 21 chromosomes of Renan (y axis) with the Chinese
746 Spring RefSeq v2.1 assembly (x axis).

747

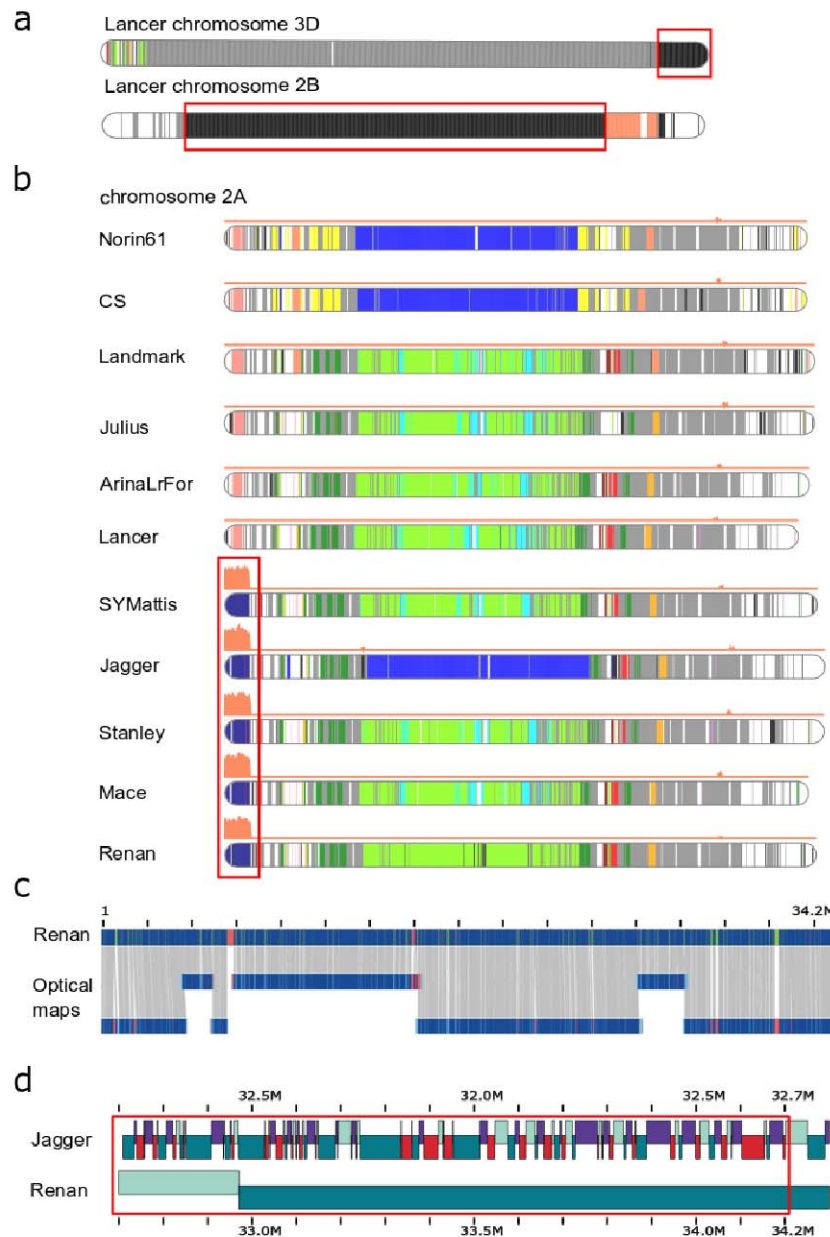


748 **Figure 4.** Representation of haplotype blocks in chromosome 6A for the 11 chromosome-
749 scale cultivars (based on 1-Mbp blocks). Regions with the same colour represent common
750 regions in wheat lines, except white regions which are not contained in haplotype blocks.
751 The gray and black regions represent haplotypes respectively shared by at least 10 cultivars
752 or specific to a given cultivar.
753



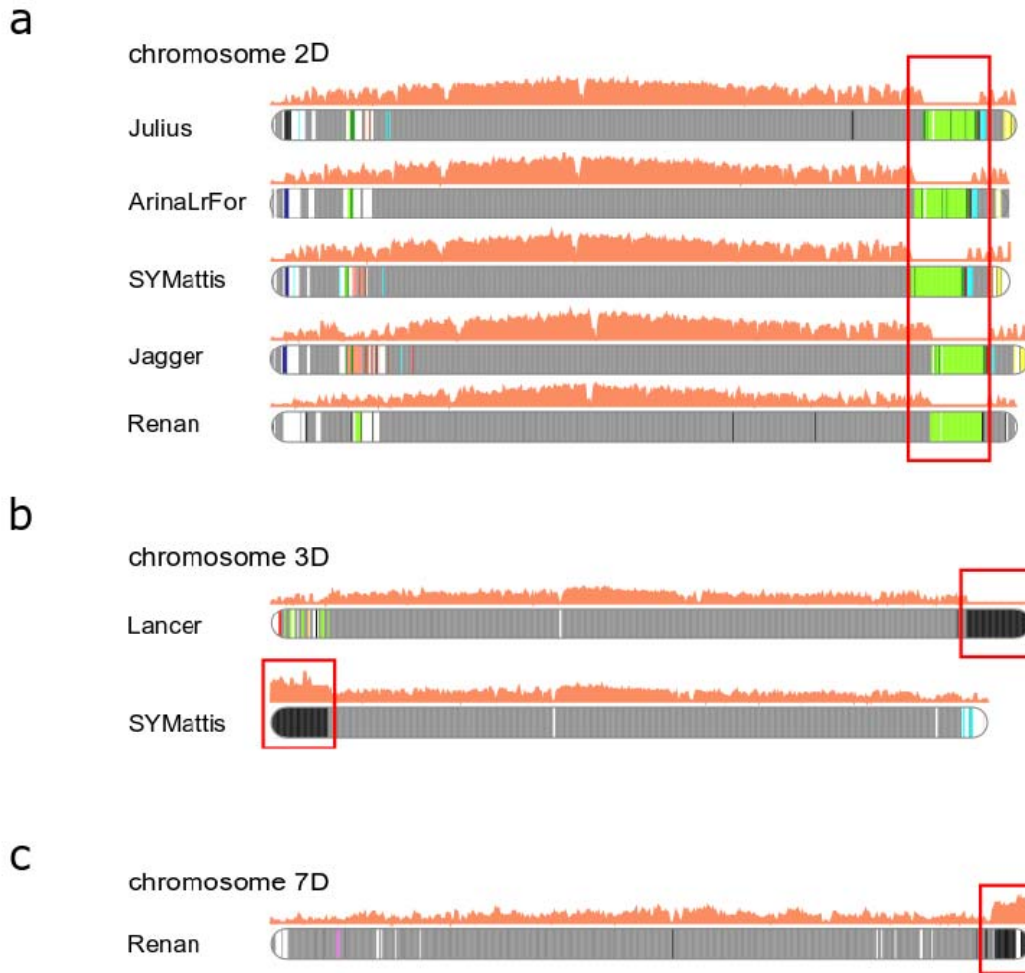
754 **Figure 5.** Haplotypic blocks in wheat chromosomes. Colors represent common regions in
755 wheat cultivars. The gray and black regions represent haplotypes respectively shared by at
756 least 10 cultivars or specific to a given cultivar. The orange curve, when present, represents
757 coverage with *Ae. ventricosa* short reads. The red boxes frame the introgressions. **a.** Known
758 introgressions in chromosomes 3D and 2B in Lancer. Regions in black represent genomic
759 regions that are specific to Lancer and are respectively *T. ponticum* and *T. timopheevii*
760 introgressions as described previously[8]. **b.** *Ae. ventricosa* introgression on chromosome
761 3D in Stanley, Mace, SY Mattis and Jagger. This known introgression is also present in
762 Renan. The dark blue block represents the region shared across the five cultivars. **c.**
763 Validation of the introgression in Renan (chromosome 2A from 1 to 34.2Mb) using Bionano
764 maps. **d.** Comparison of the contig composition of the first megabases from the introgression

765 point
766 and



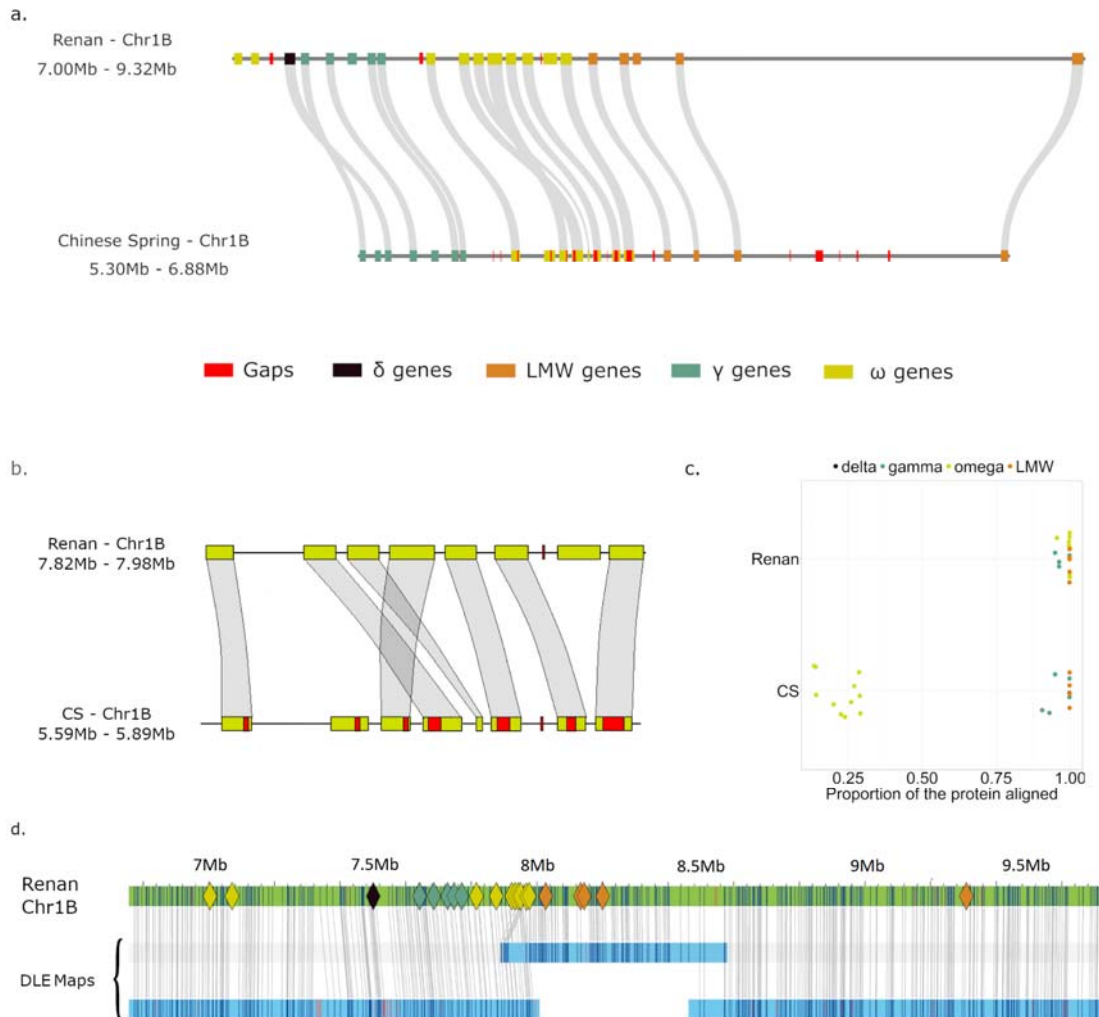
in Jagger
Renan
cultivars.

768 **Figure 6.** Haplotypic blocks in wheat chromosomes. Colors represent common regions in
769 wheat cultivars. The gray and black regions represent haplotypes respectively shared by at
770 least 10 cultivars or specific to a given cultivar. The orange curve represents coverage with
771 *Ae. ventricosa* short reads. The red boxes frame the introgressions. **a.** Candidate
772 introgression (green block) on chromosomes 2D in Julius, ArinaLrFor, SY Mattis, Jagger and
773 Renan. **b.** Candidate introgressions (black blocks) on chromosome 3D in Lancer and SY
774 Mattis. **c.** *Ae. ventricosa* introgression (black block) on chromosome 7D in Renan.



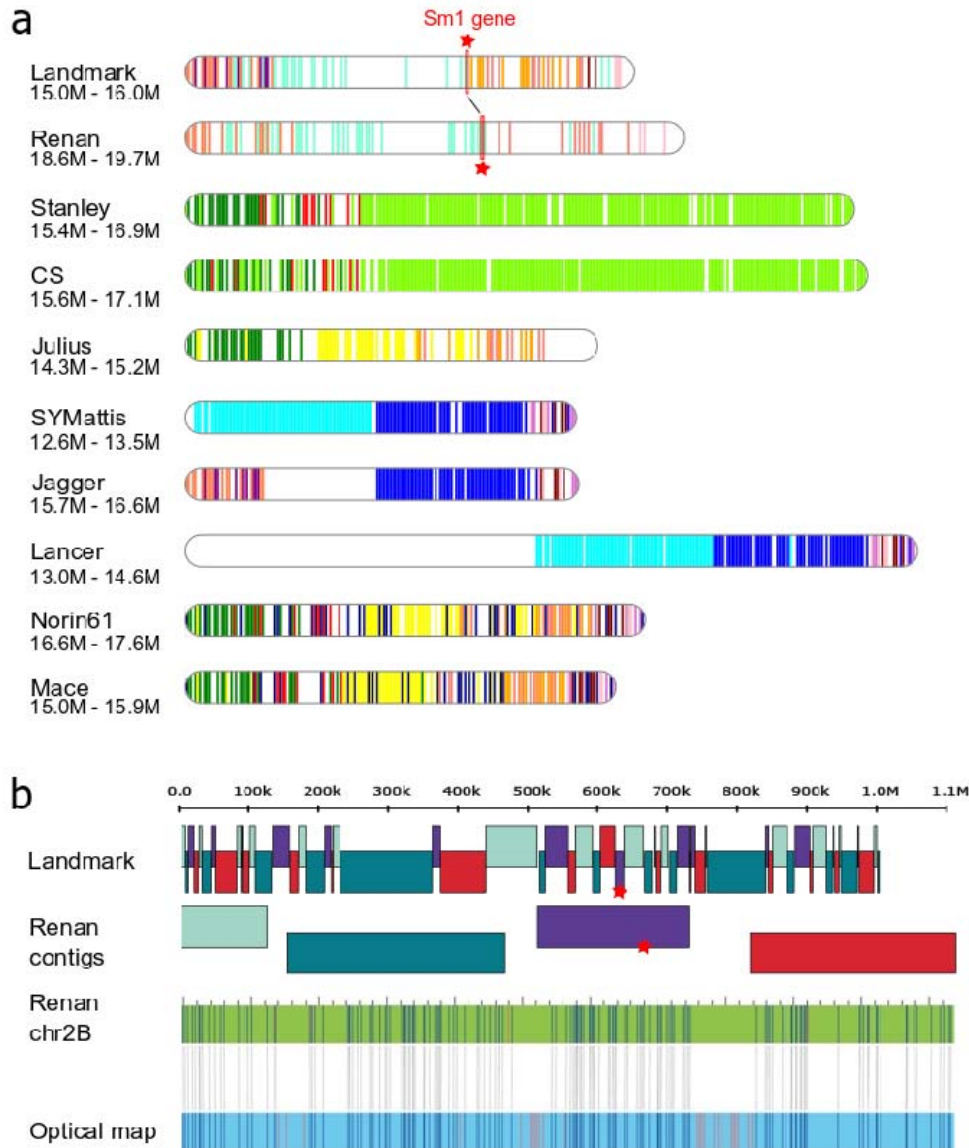
775

776 **Figure 7.** Comparative view of an important locus on chromosome 1B containing prolamin
777 and resistance genes, tandemly duplicated. **a.** Representation of the region with gaps and
778 genes on the two assemblies of Renan and CS. **b.** Zoomed view on the omega gliadin gene
779 cluster **c.** Proportion of the length of the proteins that were aligned in the genomic region of
780 Renan and CS. **d.** Alignment view of Bionano maps on the Renan cluster, colored diamond
781 shapes represent genes belonging to the omega gliadin gene cluster. The optical maps are
782 in blue and the chromosome sequence in green. Restriction sites are represented by vertical
783 lines and are joined between the sequence and the map when properly aligned.



784
785

786 **Figure 8.** Comparison of the *Sm1* loci. **a.** Representation of haplotype blocks (5kb bins) of
787 the region surrounding the *Sm1* gene on chromosome 2B. Colors represent common
788 regions in wheat cultivars. The genomic region of Landmark (15Mb to 16Mb) was aligned
789 against other cultivars to localize the *Sm1* loci. The *Sm1* gene in Landmark and Renan, the
790 two *Sm1* carrier cultivars, is represented by a red star. **b.** Comparison of the contig
791 composition in the *Sm1* region of Landmark and Renan, and validation of the assembly
792 structure in Renan using Bionano optical maps. The optical map is in blue and the
793 chromosome sequence in green. Restriction sites are represented by vertical lines and are
794 joined between the sequence and the map when properly aligned..



796 References

- 797 1. Dubcovsky J, Dvorak J. Genome Plasticity a Key Factor in the Success of Polyploid
798 Wheat Under Domestication. *Science*. American Association for the Advancement of
799 Science; 2007; doi: 10.1126/science.1143986.
- 800 2. Marcussen T, Sandve SR, Heier L, Spannagl M, Pfeifer M, International Wheat Genome
801 Sequencing Consortium, et al.. Ancient hybridizations among the ancestral genomes of
802 bread wheat. *Science*. 2014; doi: 10.1126/science.1250092.
- 803 3. Guan J, Garcia DF, Zhou Y, Appels R, Li A, Mao L. The Battle to Sequence the Bread
804 Wheat Genome: A Tale of the Three Kingdoms. *Genomics Proteomics Bioinformatics*. 2020;
805 doi: 10.1016/j.gpb.2019.09.005.
- 806 4. Chapman JA, Mascher M, Buluç A, Barry K, Georganas E, Session A, et al.. A whole-
807 genome shotgun approach for assembling and anchoring the hexaploid bread wheat
808 genome. *Genome Biol*. 2015; doi: 10.1186/s13059-015-0582-8.
- 809 5. Zimin AV, Puiu D, Hall R, Kingan S, Clavijo BJ, Salzberg SL. The first near-complete
810 assembly of the hexaploid bread wheat genome, *Triticum aestivum*. *GigaScience*. 2017; doi:
811 10.1093/gigascience/gix097.
- 812 6. Clavijo BJ, Venturini L, Schudoma C, Accinelli GG, Kaithakottil G, Wright J, et al.. An
813 improved assembly and annotation of the allohexaploid wheat genome identifies complete
814 families of agronomic genes and provides genomic evidence for chromosomal
815 translocations. *Genome Res*. 2017; doi: 10.1101/gr.217117.116.
- 816 7. Consortium (IWGSC) TIWGS, Appels R, Eversole K, Stein N, Feuillet C, Keller B, et al..
817 Shifting the limits in wheat research and breeding using a fully annotated reference genome.
818 *Science*. American Association for the Advancement of Science; 2018; doi:
819 10.1126/science.aar7191.
- 820 8. Walkowiak S, Gao L, Monat C, Haberer G, Kassa MT, Brinton J, et al.. Multiple wheat
821 genomes reveal global variation in modern breeding. *Nature*. 2020; doi: 10.1038/s41586-
822 020-2961-x.
- 823 9. Miga KH, Koren S, Rhie A, Vollger MR, Gershman A, Bzikadze A, et al.. Telomere-to-
824 telomere assembly of a complete human X chromosome. *Nature*. 2020; doi:
825 10.1038/s41586-020-2547-7.
- 826 10. Belser C, Istace B, Denis E, Dubarry M, Baurens F-C, Falentin C, et al.. Chromosome-
827 scale assemblies of plant genomes using nanopore long reads and optical maps. *Nat Plants*.
828 Nature Publishing Group; 2018; doi: 10.1038/s41477-018-0289-4.
- 829 11. Rousseau-Gueutin M, Belser C, Da Silva C, Richard G, Istace B, Cruaud C, et al.. Long-
830 read assembly of the *Brassica napus* reference genome Darmor-bzh. *GigaScience*. 2020;
831 doi: 10.1093/gigascience/giaa137.
- 832 12. Li G, Wang L, Yang J, He H, Jin H, Li X, et al.. A high-quality genome assembly
833 highlights rye genomic characteristics and agronomically important genes. *Nat Genet*. 2021;
834 doi: 10.1038/s41588-021-00808-z.
- 835 13. Liu J, Seetharam AS, Chougule K, Ou S, Swentowsky KW, Gent JI, et al.. Gapless
836 assembly of maize chromosomes using long-read technologies. *Genome Biol*. 2020; doi:
837 10.1186/s13059-020-02029-9.
- 838 14. Tørresen OK, Star B, Mier P, Andrade-Navarro MA, Bateman A, Jarnot P, et al.. Tandem
839 repeats lead to sequence assembly errors and impose multi-level challenges for genome
840 and protein databases. *Nucleic Acids Res*. 2019; doi: 10.1093/nar/gkz841.
- 841 15. Li C, Xiang X, Huang Y, Zhou Y, An D, Dong J, et al.. Long-read sequencing reveals
842 genomic structural variations that underlie creation of quality protein maize. *Nat Commun*.
843 Nature Publishing Group; 2020; doi: 10.1038/s41467-019-14023-2.
- 844 16. Ruan J, Li H. Fast and accurate long-read assembly with wtdbg2. *Nat Methods*. Nature
845 Publishing Group; 2020; doi: 10.1038/s41592-019-0669-3.
- 846 17. Liu H, Wu S, Li A, Ruan J. SMARTdenovo: a de novo assembler using long noisy reads.
847 *Gigabyte*. GigaScience Press; 2021; doi: 10.46471/gigabyte.15.
- 848 18. Kolmogorov M, Yuan J, Lin Y, Pevzner PA. Assembly of long, error-prone reads using

- 849 repeat graphs. *Nat Biotechnol.* Nature Publishing Group; 2019; doi: 10.1038/s41587-019-
850 0072-8.
- 851 19. Vaser R, Sović I, Nagarajan N, Šikić M. Fast and accurate de novo genome assembly
852 from long uncorrected reads. *Genome Res.* 2017; doi: 10.1101/gr.214270.116.
- 853 20. Aury J-M, Istace B. Hapo-G, haplotype-aware polishing of genome assemblies with
854 accurate reads. *NAR Genomics Bioinforma.* 2021; doi: 10.1093/nargab/lqab034.
- 855 21. Istace B, Belser C, Aury J-M. BiSCoT: improving large eukaryotic genome assemblies
856 with optical maps. *PeerJ.* PeerJ Inc.; 2020; doi: 10.7717/peerj.10150.
- 857 22. Zhu T, Wang L, Rimbart H, Rodriguez JC, Deal KR, Oliveira RD, et al.. Optical maps
858 refine the bread wheat *Triticum aestivum* cv. Chinese Spring genome assembly. *Plant J.*
859 2021; doi: 10.1111/tpj.15289.
- 860 23. Rimbart H, Darrier B, Navarro J, Kitt J, Choulet F, Leveugle M, et al.. High throughput
861 SNP discovery and genotyping in hexaploid wheat. *PLOS ONE.* Public Library of Science;
862 2018; doi: 10.1371/journal.pone.0186329.
- 863 24. Istace B, Belser C, Falentin C, Labadie K, Boideau F, Deniot G, et al.. Sequencing and
864 Chromosome-Scale Assembly of Plant Genomes, *Brassica rapa* as a Use Case. *Biology.*
865 Multidisciplinary Digital Publishing Institute; 2021; doi: 10.3390/biology10080732.
- 866 25. Altschul SF, Gish W, Miller W, Myers EW, Lipman DJ. Basic local alignment search tool.
867 *J Mol Biol.* 1990; doi: 10.1016/S0022-2836(05)80360-2.
- 868 26. De Oliveira R, Rimbart H, Balfourier F, Kitt J, Dynamant E, Vrána J, et al.. Structural
869 Variations Affecting Genes and Transposable Elements of Chromosome 3B in Wheats.
870 *Front Genet.* Frontiers; 2020; doi: 10.3389/fgene.2020.00891.
- 871 27. Wick RR, Judd LM, Holt KE. Performance of neural network basecalling tools for Oxford
872 Nanopore sequencing. *Genome Biol.* 2019; doi: 10.1186/s13059-019-1727-y.
- 873 28. Daron J, Glover N, Pingault L, Theil S, Jamilloux V, Paux E, et al.. Organization and
874 evolution of transposable elements along the bread wheat chromosome 3B. *Genome Biol.*
875 2014; doi: 10.1186/s13059-014-0546-4.
- 876 29. Wicker T, Gundlach H, Spannagl M, Uauy C, Borrill P, Ramírez-González RH, et al..
877 Impact of transposable elements on genome structure and evolution in bread wheat.
878 *Genome Biol.* 2018; doi: 10.1186/s13059-018-1479-0.
- 879 30. Leroy P, Guilhot N, Sakai H, Bernard A, Choulet F, Theil S, et al.. TriAnnot: A Versatile
880 and High Performance Pipeline for the Automated Annotation of Plant Genomes. *Front Plant*
881 *Sci.* Frontiers; 2012; doi: 10.3389/fpls.2012.00005.
- 882 31. Brinton J, Ramirez-Gonzalez RH, Simmonds J, Wingen L, Orford S, Griffiths S, et al.. A
883 haplotype-led approach to increase the precision of wheat breeding. *Commun Biol.* 2020;
884 doi: 10.1038/s42003-020-01413-2.
- 885 32. Hao M, Zhang L, Ning S, Huang L, Yuan Z, Wu B, et al.. The Resurgence of
886 Introgression Breeding, as Exemplified in Wheat Improvement. *Front Plant Sci.* 2020; doi:
887 10.3389/fpls.2020.00252.
- 888 33. Kondrashov FA. Gene duplication as a mechanism of genomic adaptation to a changing
889 environment. *Proc R Soc B Biol Sci.* Royal Society; 2012; doi: 10.1098/rspb.2012.1108.
- 890 34. Panchy N, Lehti-Shiu M, Shiu S-H. Evolution of Gene Duplication in Plants. *Plant*
891 *Physiol.* 2016; doi: 10.1104/pp.16.00523.
- 892 35. Huo N, Zhang S, Zhu T, Dong L, Wang Y, Mohr T, et al.. Gene Duplication and Evolution
893 Dynamics in the Homeologous Regions Harboring Multiple Prolamin and Resistance Gene
894 Families in Hexaploid Wheat. *Front Plant Sci.* Frontiers; 2018; doi: 10.3389/fpls.2018.00673.
- 895 36. Xu J-H, Messing J. Organization of the prolamin gene family provides insight into the
896 evolution of the maize genome and gene duplications in grass species. *Proc Natl Acad Sci U*
897 *S A.* 2008; doi: 10.1073/pnas.0807026105.
- 898 37. Lang D, Zhang S, Ren P, Liang F, Sun Z, Meng G, et al.. Comparison of the two up-to-
899 date sequencing technologies for genome assembly: HiFi reads of Pacific Biosciences
900 Sequel II system and ultralong reads of Oxford Nanopore. *GigaScience.* 2020; doi:
901 10.1093/gigascience/giaa123.
- 902 38. Hon T, Mars K, Young G, Tsai Y-C, Karalius JW, Landolin JM, et al.. Highly accurate
903 long-read HiFi sequencing data for five complex genomes. *Sci Data.* 2020; doi:

- 904 10.1038/s41597-020-00743-4.
- 905 39. Belser C, Baurens F-C, Noel B, Martin G, Cruaud C, Istace B, et al.. Telomere-to-
906 telomere gapless chromosomes of banana using nanopore sequencing. *Commun Biol*.
907 2021; doi: 10.1038/s42003-021-02559-3.
- 908 40. Lv X, Chen Z, Lu Y, Yang Y. An End-to-end Oxford Nanopore Basecaller Using
909 Convolution-augmented Transformer. 2020 Nov.
- 910 41. Huang N, Nie F, Ni P, Luo F, Wang J. An attention-based neural network basecaller for
911 Oxford Nanopore sequencing data. *2019 IEEE Int Conf Bioinforma Biomed BIBM*.
- 912 42. Alberti A, Poulain J, Engelen S, Labadie K, Romac S, Ferrera I, et al.. Viral to metazoan
913 marine plankton nucleotide sequences from the Tara Oceans expedition. *Sci Data*. Nature
914 Publishing Group; 2017; doi: 10.1038/sdata.2017.93.
- 915 43. Rhie A, Walenz BP, Koren S, Phillippy AM. Merqury: reference-free quality,
916 completeness, and phasing assessment for genome assemblies. *Genome Biol*. 2020; doi:
917 10.1186/s13059-020-02134-9.
- 918 44. Durand NC, Shamim MS, Machol I, Rao SSP, Huntley MH, Lander ES, et al.. Juicer
919 Provides a One-Click System for Analyzing Loop-Resolution Hi-C Experiments. *Cell Syst*.
920 2016; doi: 10.1016/j.cels.2016.07.002.
- 921 45. Dudchenko O, Batra SS, Omer AD, Nyquist SK, Hoeger M, Durand NC, et al.. De novo
922 assembly of the *Aedes aegypti* genome using Hi-C yields chromosome-length scaffolds.
923 *Science*. American Association for the Advancement of Science; 2017; doi:
924 10.1126/science.aal3327.
- 925 46. Pedersen BS, Quinlan AR. Mosdepth: quick coverage calculation for genomes and
926 exomes. *Bioinforma Oxf Engl*. 2018; doi: 10.1093/bioinformatics/btx699.
- 927 47. Abyzov A, Urban AE, Snyder M, Gerstein M. CNVnator: an approach to discover,
928 genotype, and characterize typical and atypical CNVs from family and population genome
929 sequencing. *Genome Res*. 2011; doi: 10.1101/gr.114876.110.
- 930 48. Kent WJ. BLAT—The BLAST-Like Alignment Tool. *Genome Res*. 2002; doi:
931 10.1101/gr.229202.
- 932 49. Wu TD, Watanabe CK. GMAP: a genomic mapping and alignment program for mRNA
933 and EST sequences. *Bioinformatics*. 2005; doi: 10.1093/bioinformatics/bti310.
- 934 50. Quinlan AR, Hall IM. BEDTools: a flexible suite of utilities for comparing genomic
935 features. *Bioinformatics*. 2010; doi: 10.1093/bioinformatics/btq033.
- 936 51. Kim D, Paggi JM, Park C, Bennett C, Salzberg SL. Graph-based genome alignment and
937 genotyping with HISAT2 and HISAT-genotype. *Nat Biotechnol*. 2019; doi: 10.1038/s41587-
938 019-0201-4.
- 939 52. Pertea M, Pertea GM, Antonescu CM, Chang T-C, Mendell JT, Salzberg SL. StringTie
940 enables improved reconstruction of a transcriptome from RNA-seq reads. *Nat Biotechnol*.
941 2015; doi: 10.1038/nbt.3122.
- 942 53. Trapnell C, Williams BA, Pertea G, Mortazavi A, Kwan G, van Baren MJ, et al..
943 Transcript assembly and quantification by RNA-Seq reveals unannotated transcripts and
944 isoform switching during cell differentiation. *Nat Biotechnol*. 2010; doi: 10.1038/nbt.1621.
- 945 54. Holley G, Melsted P. Bifrost: highly parallel construction and indexing of colored and
946 compacted de Bruijn graphs. *Genome Biol*. 2020; doi: 10.1186/s13059-020-02135-8.
- 947 55. Hao Z, Lv D, Ge Y, Shi J, Weijers D, Yu G, et al.. Rldeogram: drawing SVG graphics to
948 visualize and map genome-wide data on the idiograms. *PeerJ Comput Sci*. PeerJ Inc.; 2020;
949 doi: 10.7717/peerj-cs.251.
- 950 56. Tang H, Bowers JE, Wang X, Ming R, Alam M, Paterson AH. Synteny and Collinearity in
951 Plant Genomes. *Science*. American Association for the Advancement of Science; 2008; doi:
952 10.1126/science.1153917.
- 953 57. Zulkower V, Rosser S. DNA Features Viewer, a sequence annotations formatting and
954 plotting library for Python. *bioRxiv*. Cold Spring Harbor Laboratory; 2020; doi:
955 10.1101/2020.01.09.900589.
- 956